

# Review of COVID-19 Antibody Therapies

Jiahui Chen<sup>1</sup>, Kaifu Gao<sup>1\*</sup>, Rui Wang<sup>1</sup>, Duc Duy Nguyen<sup>2</sup>, and Guo-Wei Wei<sup>1,3,4†</sup>

<sup>1</sup> Department of Mathematics,  
Michigan State University, MI 48824, USA.

<sup>2</sup> Department of Mathematics,  
University of Kentucky, KY 40506, USA.

<sup>3</sup> Department of Electrical and Computer Engineering,  
Michigan State University, MI 48824, USA.

<sup>4</sup> Department of Biochemistry and Molecular Biology,  
Michigan State University, MI 48824, USA.

June 19, 2020

## Abstract

Under the global health emergency caused by coronavirus disease 2019 (COVID-19), efficient and specific therapies are urgently needed. Compared with traditional small-molecular drugs, antibody therapies are relatively easy to develop and as specific as vaccines in targeting severe acute respiratory syndrome coronavirus 2 (SARS-CoV-2), and thus attract much attention in the past few months. This work reviews seven existing antibodies for SARS-CoV-2 spike (S) protein with three-dimensional (3D) structures deposited in the Protein Data Bank. Five antibody structures associated with SARS-CoV are evaluated for their potential in neutralizing SARS-CoV-2. The interactions of these antibodies with the S protein receptor-binding domain (RBD) are compared with those of angiotensin-converting enzyme 2 (ACE2) and RBD complexes. Due to the orders of magnitude in the discrepancies of experimental binding affinities, we introduce topological data analysis (TDA), a variety of network models, and deep learning to analyze the binding strength and therapeutic potential of the aforementioned fourteen antibody-antigen complexes. The current COVID-19 antibody clinical trials, which are not limited to the S protein target, are also reviewed.

Key words: COVID-19, SARS-CoV-2, antibody therapy, binding affinity, persistent homology, deep learning, network analysis.

---

\*Jiahui Chen and Kaifu Gao contributed equally.

†Corresponding author. Email: wei@math.msu.edu

# Introduction

Coronavirus disease 2019 (COVID-19) pandemic caused by severe acute respiratory syndrome coronavirus 2 (SARS-CoV-2) has rapidly spread around the world. By June 17, 2020, more than 8.2 million individuals were infected and 443,000 fatalities had been reported. Currently, there are neither specific drugs nor effective vaccines available [7]. Traditional drug discovery involves a long and costly process, requiring more than 10 years to put an average drug on the market. Vaccine development typically takes more than one year. In contrast, developing potent SARS-CoV-2 specified antibodies that are produced from blood B cells in response to and counteracting SARS-CoV-2 antigens is a less time-consuming and more efficient strategy for combating the ongoing pandemic [7, 29, 34, 47, 54, 62, 70, 71, 78, 82, 85].

Antibody (Ab), also called immunoglobulin (Ig), is a large, Y-shaped protein that typically consists of two identical heavy chains and two identical light chains. A heavy chain can be separated into two regions, the constant region and the variable region. Moreover, each light chain has two successive domains, the constant domain and the variable domain. The two heavy and two light chains of an antibody are connected through disulfide bonds within the constant region [50]. An antibody binds the antigenic determinant (also called epitope) through the variable regions in the tips of the heavy and light chains. Each of these chains contains three complementarity determining regions (CDRs), which located in the tips of each variable domain. Most of the diversities between antibodies are generated within the CDRs, which determine the specificity of individuals of antibodies.

Benefit from the broad specificity of antibodies; antibody therapies have been proven to be a promising way to fight against cancer, autoimmune disease, neurological disorders, and infectious viruses such as HIV, Ebola, and Middle Eastern respiratory syndrome (MERS) [10, 56, 73]. Recently, several studies have shown that the convalescent plasma of SARS-CoV-2 patients, which contains neutralizing antibodies created by the adaptive immune response, can effectively improve patient survival rate [6, 8, 57]. However, plasma-based therapeutics cannot be produced on a large scale. Therefore, seeking potent industrial-scale antibody therapies becomes one of the most feasible strategies to fight against SARS-CoV-2. The spike (S) protein, a multi-functional molecular machine that binds the human cell receptor angiotensin-converting enzyme 2 (ACE2), has been taking as the target of neutralizing antibodies and the focus of therapeutic and vaccine design efforts [64]. Many researchers have reported the binding affinities of SARS-CoV-2 S protein in complex with antibody candidates and ACE2. However, these reported values may vary by two orders of magnitude for a given antibody due to different experimental methods, conditions, calibrations, and human errors, which hinders the development of antibody therapies for SARS-CoV-2. Therefore, developing a unified paradigm for ranking the potency of SARS-CoV-2 antibodies is a pressing need.

In this work, we review seven existing SARS-CoV-2 antibody therapeutic candidates in the literature. As molecular structures are able to reveal the molecular mechanism of antibody-antigen interactions, we only focus on the SARS-CoV-2 S protein antibodies that have three-dimensional (3D) structures released on the Protein Data Bank (PDB). Since antibodies may directly compete with ACE2 for binding to the S protein receptor-binding domain (RBD), the structure and binding affinity of ACE2 and S protein complexes are studied to understand the efficiency of antibodies. Moreover, since the S proteins of SARS-CoV and SARS-CoV-2 share 80% amino acid sequence identity [67], SARS-CoV S protein antibodies potential candidates for COVID-19. Therefore, we review five existing SARS-CoV S protein antibodies and analyze their binding affinities with the SARS-CoV-2 S protein. Furthermore, we employ topological data analysis (TDA), artificial intelligence (AI), and a variety of network models to address literature controversy and provide a unified paradigm for ranking the potency of all antibodies. Finally, we review the clinical trials of COVID-19 antibody candidates.

# 1 An overview of antibody structures, functions, and therapies

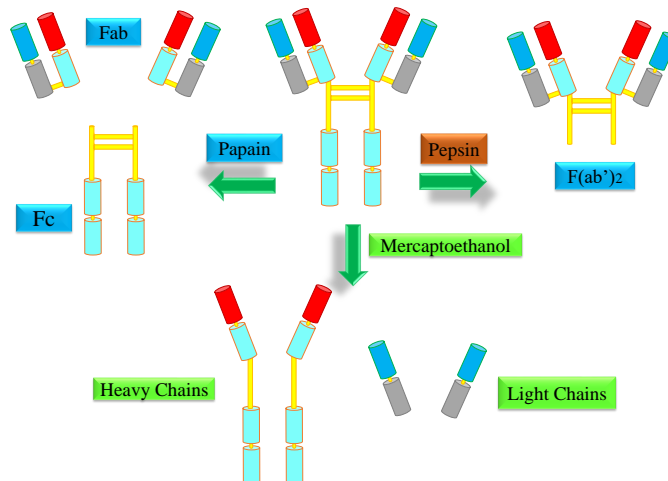


Figure 1: A schematic illustration of antibody.

An antibody can be divided into different parts according to its functions. Specifically, the “arms” of the Y-shaped protein contain sites that can recognize and bind to specific antigens. This region of the antibody is called a Fab (fragment, antigen-binding) region and composed of one constant domain and one variable domain from each heavy (VL) and light chain (VH) of the antibody [50]. Figure 1 illustrates the structure of the antibody. The variable domain (Fv region) is the most important region for binding to antigens. To be specific, on light and heavy chains, complementarity-determining regions (CDRs) composed of three variable loops of  $\beta$ -strands are responsible for binding to a specific antigen. The CDRs are incredibly variable, allowing a large number of antibodies with slightly different tip structures, or antigen-binding sites, to exist. Each of these variants can bind to a different antigen so that the enormous diversity of antibody paratopes on the antigen-binding fragments allows the immune system to recognize an equally wide variety of antigens [41]. This antibody paratope diversity is generated by random recombination events of a set of gene segments that encode different antigen-binding sites (or paratopes), followed by random mutations in this area of the antibody gene to create further diversity [14,40]. It has been estimated that humans generate about 10 billion different antibodies [22]. The base of the Y plays a role in modulating immune cell activity. This region is named an Fc (Fragment, crystallizable) region and is composed of two heavy chains. The Fc region ensures each antibody generates an appropriate immune response for a given antigen, by binding to a specific class of Fc receptors or other immune molecules. This process activates different physiological effects, including recognition of opsonized particles, lysis of cells, and degranulation of mast cells, basophils, and eosinophils [31,77].

In addition to conventional antibodies, camelids also produce heavy-chain-only antibodies (HCAbs). HCAbs, also referred to as VHVs, or nanobodies, contain a single variable domain (VHH) that makes up the equivalent antigen-binding fragment (Fab) of conventional immunoglobulin G (IgG) antibodies [27]. This single variable domain typically can acquire affinity and specificity for antigens comparable to conventional antibodies. VHVs can easily be constructed into multivalent formats and have higher thermal stability and chemostability than most antibodies do [12, 15, 25, 38, 55, 65]. Another advantage of VHVs is that they are less susceptible to steric hindrances than larger conventional antibodies [23].

In immune systems, antibodies are generated and secreted by B cells, mostly differentiated B cells, including plasma cells or memory B cells. Antibodies have two physical forms, a membrane-bound form called the B-cell receptor (BCR), which is found to attach to the surface of B cells, and a soluble form that moves freely in the blood plasma. The BCR facilitates the activation and subsequent differentiation of B cells

into either plasma or memory B cells. The activation of B cells has two mechanisms: T cell-dependent (TD) activation and T cell-independent (TI) activation [42]. In the TD activation, once a BCR binds a TD antigen, the antigen is taken up into the B cell through receptor-mediated endocytosis, degraded, and presented to T helper (TH) cells as peptide pieces in complex with major histocompatibility complex-II (MHC-II) molecules on the cell membrane [1]. TH cells recognize and bind these MHC-II-peptide complexes through their T cell receptor (TCR). Following TCR-MHC-II-peptide binding, T cells express the surface protein CD40L as well as cytokines such as IL-4 and IL-21. These signals promote B cell proliferation, immunoglobulin class switching, somatic hypermutation, and guide differentiation. Once receiving these signals, B cells are activated [11]. In the TI activation, T cells are absent and B cells receive signals from recognition and binding of a common microbial constituent to toll-like receptors (TLRs) or extensive crosslinking of BCRs to repeated epitopes on a bacterial cell [42]. The TI activation is rapid, but antibodies generated from it tend to have a lower affinity and are also less functionally versatile than those from TD activation [42]. After activated, B cells can be differentiated into plasma cells or memory B cells to generate and secrete antibodies. Memory B cells can even survive in a human body for years to remember the same antigen and trigger a fast response upon future exposure [3].

Antibodies protect our health in four ways: first, their Fab regions can bind to pathogens, so that prevent pathogens from entering or damaging cells; second, they trigger the removal of pathogens by macrophages and other cells by coating the pathogen; third, they stimulate the destruction of pathogens by stimulating other immune responses such as the complement pathway [51]; at last, antibodies can also lead to vasoactive amine degranulation against certain types of antigens such as helminths and allergens [31].

The antibody mechanism enlightens the development of vaccines and antibody therapies. A vaccine is typically made of weakened or killed forms of the microbe, its toxins, or one of its surface proteins that resemble a disease-causing microorganism. These forms cannot cause an infection, but the immune system still regards them as a foreign object and produces antibodies in response. After the threat has passed, most of the antibodies will break down, but memory B cells remain and remember the antigens in the vaccine.

Antibody therapies were developed in the 1970s, following the discovery of the structures of antibodies and the development of hybridoma technology, which provided the first reliable source of monoclonal antibodies (mAbs) [4, 36]. Rather than extracted from convalescent patient plasma, mAbs are made from identical immune cells that are all clones of a unique parent cell so that they can have a monovalent affinity to the same epitope. As a result, the most significant advantage of mAbs over conventional small-molecular drugs is their high specificity, which facilitates precise action [30]. The second advantage is their long half-lives, which allows infrequent dosing [39]. Third, molecular engineering technologies have enabled the structure of mAbs to be fine-tuned for specific therapeutic actions and to minimize immunogenicity [26, 44, 49, 66], thus enhancing their safety. This is reflected in mAbs having an approval rate of around 20% compared with 5% for new small-molecular entities [52, 53]. Finally, mAbs can be developed in a short time period, such as 5-6 months [35]. Currently, mAbs have already established their therapeutic and prophylactic efficacy against cancer, autoimmune disease, neurological disorders, and infectious viruses such as HIV, Ebola, and Middle Eastern respiratory syndrome (MERS) [10, 56, 73]. However, adverse effects are mostly relating to immunomodulation and infection can be associated with therapeutic mAbs [30], such as antibody-dependent enhancement [63] and cytokine storm [9].

## 2 SARS-CoV-2 antibody therapeutic candidates

Both SARS-CoV and SARS-CoV-2 belong to lineage B of the betacoronavirus genus and have four structural proteins, known as spike, envelope, membrane, and nucleocapsid proteins [81, 86]. The nucleocapsid protein holds the RNA genome. Together with membrane, spike, envelope, and membrane proteins create the

viral envelope [80]. Among them, the S protein that forms homotrimers protruding from the viral surface mediates the entry of coronaviruses into host cells when binds with ACE2 [64]. More specifically, the S protein comprises two functional subunits: the S1 that is responsible for binding to the host cell receptor and the S2 that promotes the fusion of the virus and cellular membranes [68,69].

ACE2 is a single-pass transmembrane protein with its active domain exposed on the cell surface and is expressed in the lungs and other tissues [28]. ACE2 serves as the main cell entry point for SARS-CoV and SARS-CoV-2, and some other coronaviruses [70]. Notably, the equilibrium dissociation constant ( $K_d$ ) of the binding between ACE2 and S protein has significantly increased from SARS-CoV to SARS-CoV-2 [62, 67]. Moreover, plus SARS-CoV-2 may also use basigin to assist in cell entry [72]. Therefore, SARS-CoV-2 is more infectious than SARS-CoV.

Antibody therapy is promising to fight against COVID-19. Figure 2 is a schematic illustration of antibody therapy for COVID-19. Notably, neutralizing monoclonal antibodies (mAbs) isolated from convalescent patient memory B cells provide effective intervention to SARS-CoV-2 due to their safety, scalability, and therapeutic effectiveness [6,8,57]. As S protein mediates the host cell entry, it is the target of neutralizing antibodies and the focus of therapeutic and vaccine design efforts [64].

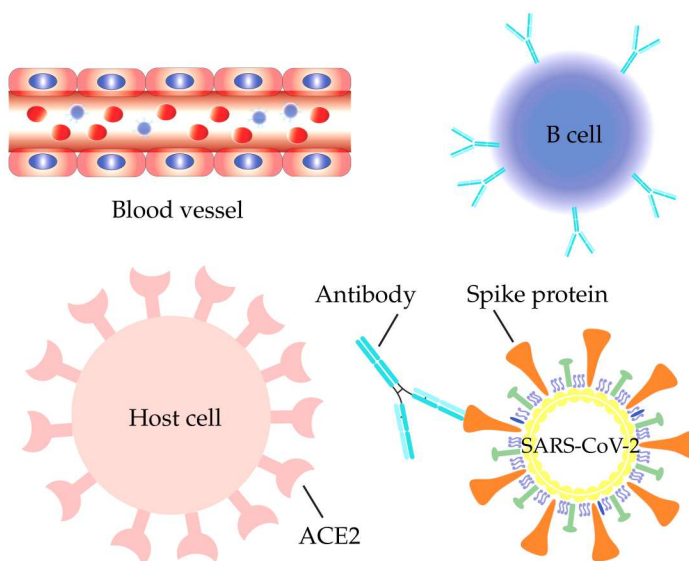


Figure 2: A schematic illustration of antibody therapy.

Table 1 provides a summary of SARS-CoV-2 and SARS-CoV S protein RBDs in complexes with existing antibodies and ACE2 structures. The structures, functions, and properties of these complexes are analyzed below.

As summarized in Table 1, twelve mAbs targeting the SARS-CoV-2 or SARS-CoV S-protein RBD are reported with their 3D experimental complex structures available in the Protein Data Bank. According to the literature reports, the most promising one is S309 [47], which shows almost equally neutralization potency against both SARS-CoV and SARS-CoV-2. The authors state that 19 out of 24 residues of the S309's epitope are strictly unchanged from SARS-CoV and SARS-CoV-2, and the other 5 residues are conservatively or semi-conservatively substituted [47]. However, some other researchers are still concerned about the claimed cross-effectiveness against both SARS-CoV and SARS-CoV-2 [71]. Notably, two experimental structures of the S309 and SARS-CoV-2 S-protein complex are released with closed and open conformations of the S-protein, respectively. The binding affinity of S309 and S protein RBD complex is not sensitive to S protein close or open conformations [47].

CR3022 is another potent antibody that may bind to both SARS-CoV and SARS-CoV-2 [62, 85]. It is

Table 1: A summary of monoclonal antibodies targeting the SARS-CoV-2 or SARS-CoV S-protein with the 3D experimental structures of their complexes available in Protein Data Bank. BLI: Biolayer interferometry, and SPR: Surface plasmon resonance.

Protein or Antibody	Target	Kd (nM) / Method	PDBID	Resolution (Å)
ACE2	SARS-CoV-2 RBD	1.2 / BLI [67] 34.6 / BLI [79] 15.2 / BLI [62]	6M0J [37]	2.45
S309	SARS-CoV-2 RBD	IgG=0.104 Fab=1.98 / BLI [47]	6WPS, 6WPT [47]	3.10, 3.70
CR3022	SARS-CoV-2 RBD	IgG=6.28 / BLI [62] IgG<0.1 Fab=115 / BLI [85]	6W41 [85]	3.08
CB6	SARS-CoV-2 RBD	IgG=2.49 / SPR [58]	7C01	2.85
P2B-2F6	SARS-CoV-2 RBD	IgG=5.14 / SPR [34]	7BWJ [34]	2.85
B38	SARS-CoV-2 RBD	IgG=70.1 / SPR [82]	7BZ5 [82]	1.84
H11-D4	SARS-CoV-2 RBD		6Z43	3.30
BD23	SARS-CoV-2 RBD		7BYR [7]	3.84
ACE2	SARS-CoV RBD	5.0 / BLI [67] 325.8 / BLI [79] 1.70 / BLI [59]	3D0G	2.80
CR3022	SARS-CoV RBD	IgG<0.1 Fab=1 / BLI [85]		
S309	SARS-CoV RBD	IgG=0.12 Fab=1.81 / BLI [47]		
m396	SARS-CoV RBD	IgG=0.005 Fab=20 / BLI [48]	2DD8 [48]	2.30
S230	SARS-CoV RBD	IgG=0.06 / BLI [70]	6NB6 [70]	4.30
VHH-72 <sup>1</sup>	SARS-CoV RBD	IgG=1.15 / SPR [78]	6WAQ [78]	2.20
80R	SARS-CoV RBD	IgG=1.59 / BLI [59]	2GHW [32]	2.30
F26G19	SARS-CoV RBD	Fab=26 / SPR [45]	3BGF [45]	3.00

also showed that compared with m396, a SARS-CoV-specific antibody, CR3022 has a significantly stronger binding signal to SARS-CoV-2. However, this affinity to SARS-CoV-2 is much weaker than the affinity to SARS-CoV [85]. It is also suggested that CR3022 can only access to the open conformation of the S-protein RBD [85].

CB6 and P2B-2F6 are also promising SARS-CoV-2 antibodies, which are specific human mAbs extracted from convalescent COVID-19 patients [34, 58]. VHH-72 cross-reacts with SARS-CoV-2 and SARS-CoV S-proteins, but the affinity to SARS-CoV-2 is much lower than SARS-CoV [78]. B38 also shows a direct competition with ACE2 for binding to SARS-CoV-2 S-protein [82].

## 2.1 3D structure alignment

All the available 3D structures of SARS-CoV-2 S protein RBD in complex of the antibodies are aligned to ACE2. Figures 3 and 4 show the alignment of SARS-CoV-2 and SARS-CoV antibodies, respectively. The PDB ID of these complexes can be found in Table 1.

As revealed in Figure 3, the antibodies CB6, B38, H11-D4, and P2B-2F6 have their epitopes overlapping with the ACE2 binding site, suggesting their bindings are in direct competition with that of ACE2. Theoretically, this direct competition reduces the viral infection rate. For an antibody with strong binding ability, it will directly neutralize SARS-CoV-2 without the need of antibody-dependent cell cytotoxicity (ADCC) and antibody-dependent cellular phagocytosis (ADCP) mechanisms. However, the binding sites of epitopes of S309 and CR3022 are away from that of ACE2, leading to the absence of binding competition [47, 62].

<sup>1</sup>The binding affinity of VHH-72 with SARS-CoV-2 RBD is Fab= 54 nM.

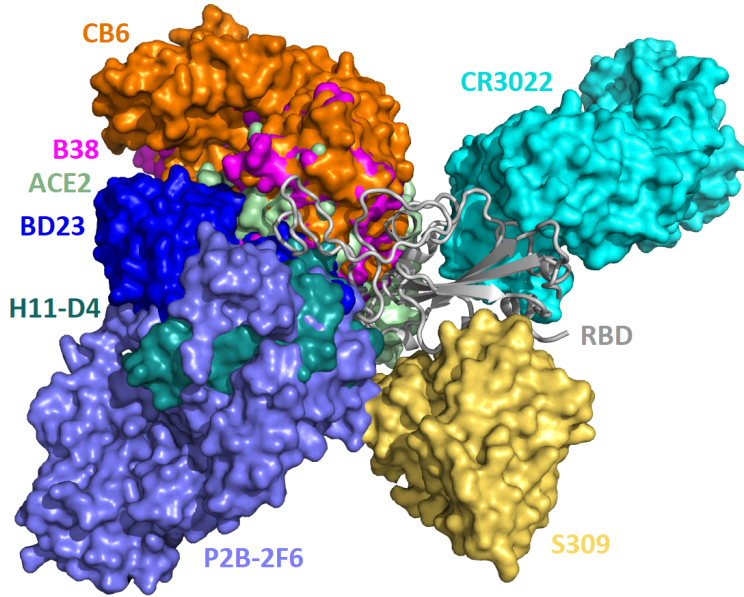


Figure 3: The alignment of the available 3D structures of SARS-CoV-2 S-protein RBD in binding complexes with antibodies as well as ACE2.

One study shows the ADCC and ADCP mechanisms contribute to the viral control conducted by S309 in infected individuals [47]. For CR3022, researches indicate that it neutralizes the virus in a synergistic fashion [60].

Figure 3 shows that on the SARS-CoV RBD, antibodies S230, 80R, F26G19, and m396 have their epitopes overlapping with ACE2. VHH-72 locates slightly away from the ACE2 binding site but still sterically clashes with the ACE2 binding. They all lead to binding-competitions to naturalize the virus.

## 2.2 Alignment of antibody and ACE2 epitopes on S protein two-dimensional (2D) sequences

Figure 5 highlights the contact regions of antibody and ACE2 epitopes on SARS-CoV-2 RBD or SARS-CoV RBD 2D sequences. Consistent with the 3D alignment, except for S309, CR3022, and VHH-72, all the other antibodies have their epitopes overlapping with the ACE2 binding site, especially the residues from 486 to 505 of the SARS-CoV-2 RBD (corresponding to the residues 472 to 491 of the SARS-CoV RBD). Although the VHH-72 epitope residues do not overlap with the ACE2 binding site, VHH72 occupies parts of the space of the ACE2 binding site, which will disrupt the ACE2 binding with RBD. Therefore, VHH-72 also has a competitive binding ability against ACE2. Figure 5 also reveals that these epitope residues have many mutations from SARS-CoV-2 RBD to SARS-CoV RBD, which could explain why most of the antibodies lack cross-reaction to both SARS-CoV-2 and SARS-CoV. This aspect will be further studied in a later section.

## 3 Experimental pitfalls in the affinity measurements of antibody binding with S protein RBD

Table 1 clearly displays the discrepancy in reported experimental  $K_d$  values for ACE2 in complexes with SARS-CoV-2 S-protein (i.e., 1.2 nM [67], 15.2 nM [62], and 34.6 nM [79]). Moreover, a 191-fold difference in



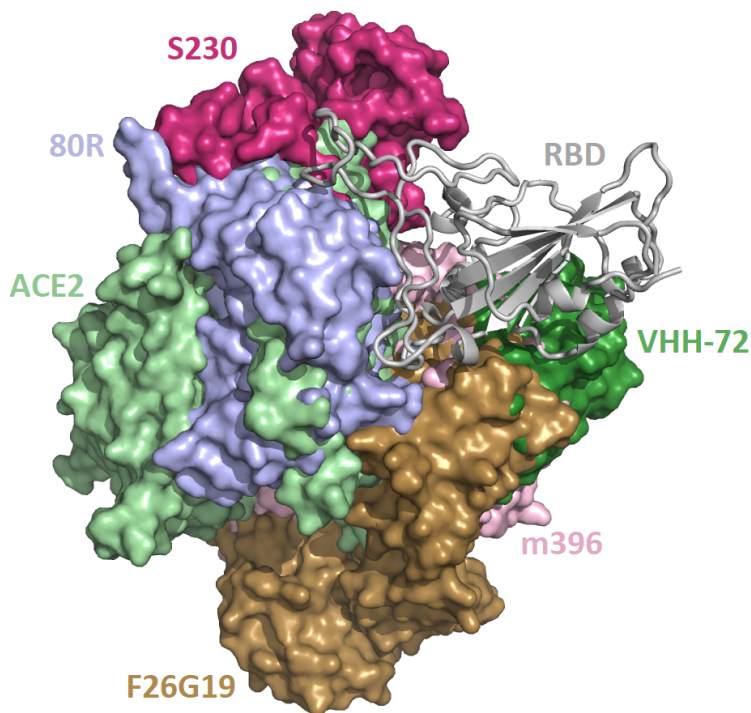


Figure 4: The alignment of the available 3D structures of SARS-CoV S-protein RBD in binding complexes with antibodies as well as ACE2.

magnitude has been reported in experimental  $K_d$  values for ACE2 and SARS-CoV S-protein complex (i.e., 5.0 nM [67], 325.8 nM [79], and 1.70 nM [59]).

The inconsistency mentioned above in experimental values is not isolated. The experimental  $K_d$  values for CR3022 binding with the SARS-CoV-2 S protein RBD were reported as 6.28 nM [62] and <0.1 nM [85]. This level of discrepancy in reported experimental values makes it impossible to select antibody candidates appropriately.

As shown in Table 1, two binding assay techniques are used to measure  $K_d$  values of antibody-antigen interactions. The discrepancies in  $K_d$  values for CR3022 discussed above are based on biolayer interferometry (BLI) measurements. BLI detects the surface changes on biosensor tips induced by protein-protein association and dissociation by using analyzing the interference pattern of white light reflected from the surface. BLI results are sensitive to biosensor preparation, the stability of the light source, the temperature control, and the calibration. Surface plasmon resonance (SPR) has been employed for determining the  $K_d$  values of antibody and RBD complexes as shown in Table 1. This method detected the reflectivity changed induced by molecular adsorption, such as polymers, DNA or proteins, etc. by changes in reflection angles. Similarly, SPR is also sensitive to the preparation of conjugated antigens, the stability of the light source, the temperature control, and the calibration. The widespread inconsistency in reported antibody and S protein binding affinities motivates us to carry out computational analysis of existing antibody-S protein complexes described below.

## 4 Computational analysis of antibody-SARS-CoV-2 interactions

To have unified assessment and ranking of S protein RBD binding complexes with antibodies and ACE2, we utilize topological data analysis, graph theory, network models, and machine learning to analyze the 3D complexes presented in Table 1. We also evaluate the re-purposing potentials of SARS-CoV antibodies



6M0J(ACE2) 319 RVQPTESIVRFPNITNLCPPGGEVFNATRFASVYAWNRRKISNCVADYSLVLYNSASFSTFKCYGVSPSTKLNLCFTNYYADSFVIRGDEVQRQ 409  
6WPS(S309) 319 RVQPTESIVRFPNITNLCPPGGEVFNATRFASVYAWNRRKISNCVADYSLVLYNSASFSTFKCYGVSPSTKLNLCFTNYYADSFVIRGDEVQRQ 409  
6W41(CR3022) 319 RVQPTESIVRFPNITNLCPPGGEVFNATRFASVYAWNRRKISNCVADYSLVLYNSASFSTFKCYGVSPSTKLNLCFTNYYADSFVIRGDEVQRQ 409  
7C01(CB7) 319 RVQPTESIVRFPNITNLCPPGGEVFNATRFASVYAWNRRKISNCVADYSLVLYNSASFSTFKCYGVSPSTKLNLCFTNYYADSFVIRGDEVQRQ 409  
7BWJ(P2B-2F6) 319 RVQPTESIVRFPNITNLCPPGGEVFNATRFASVYAWNRRKISNCVADYSLVLYNSASFSTFKCYGVSPSTKLNLCFTNYYADSFVIRGDEVQRQ 409  
7BZ5(B38) 319 RVQPTESIVRFPNITNLCPPGGEVFNATRFASVYAWNRRKISNCVADYSLVLYNSASFSTFKCYGVSPSTKLNLCFTNYYADSFVIRGDEVQRQ 409  
6Z43(H11-D4) 319 RVQPTESIVRFPNITNLCPPGGEVFNATRFASVYAWNRRKISNCVADYSLVLYNSASFSTFKCYGVSPSTKLNLCFTNYYADSFVIRGDEVQRQ 409  
7BYR(BD23) 319 RVQPTESIVRFPNITNLCPPGGEVFNATRFASVYAWNRRKISNCVADYSLVLYNSASFSTFKCYGVSPSTKLNLCFTNYYADSFVIRGDEVQRQ 409  
3D0G(ACE2) 306 RVVPSGDVVRFPNITNLCPPGGEVFNATKFPSSVYAWERKKISNCVADYSLVLYNSTFFSTFKCYGVSPSTKLNLCFTNYYADSFVIRGDEVQRQ 396  
2DD8(m396) 306 RVVPSGDVVRFPNITNLCPPGGEVFNATKFPSSVYAWERKKISNCVADYSLVLYNSTFFSTFKCYGVSPSTKLNLCFTNYYADSFVIRGDEVQRQ 396  
6NB6(S230) 306 RVVPSGDVVRFPNITNLCPPGGEVFNATKFPSSVYAWERKKISNCVADYSLVLYNSTFFSTFKCYGVSPSTKLNLCFTNYYADSFVIRGDEVQRQ 396  
6WAQ(VHH-72) 306 RVVPSGDVVRFPNITNLCPPGGEVFNATKFPSSVYAWERKKISNCVADYSLVLYNSTFFSTFKCYGVSPSTKLNLCFTNYYADSFVIRGDEVQRQ 396  
2GHW(80R) 306 RVVPSGDVVRFPNITNLCPPGGEVFNATKFPSSVYAWERKKISNCVADYSLVLYNSTFFSTFKCYGVSPSTKLNLCFTNYYADSFVIRGDEVQRQ 396  
3BGF(F26G19) 306 RVVPSGDVVRFPNITNLCPPGGEVFNATKFPSSVYAWERKKISNCVADYSLVLYNSTFFSTFKCYGVSPSTKLNLCFTNYYADSFVIRGDEVQRQ 396

6M0J(ACE2) 410 IAPGQTGKIADYNYKLPDDFTGCVI AWNSNNLDSKVGNNYLYRLFRKSNLKPFFERDI STEIYQAGSTPCNGVEGFNCYFPLQSYGFOPT 500  
6WPS(S309) 410 IAPGQTGKIADYNYKLPDDFTGCVI AWNSNNLDSKVGNNYLYRLFRKSNLKPFFERDI STEIYQAGSTPCNGVEGFNCYFPLQSYGFOPT 500  
6W41(CR3022) 410 IAPGQTGKIADYNYKLPDDFTGCVI AWNSNNLDSKVGNNYLYRLFRKSNLKPFFERDI STEIYQAGSTPCNGVEGFNCYFPLQSYGFOPT 500  
7C01(CB7) 410 IAPGQTGKIADYNYKLPDDFTGCVI AWNSNNLDSKVGNNYLYRLFRKSNLKPFFERDI STEIYQAGSTPCNGVEGFNCYFPLQSYGFOPT 500  
7BWJ(P2B-2F6) 410 IAPGQTGKIADYNYKLPDDFTGCVI AWNSNNLDSKVGNNYLYRLFRKSNLKPFFERDI STEIYQAGSTPCNGVEGFNCYFPLQSYGFOPT 500  
7BZ5(B38) 410 IAPGQTGKIADYNYKLPDDFTGCVI AWNSNNLDSKVGNNYLYRLFRKSNLKPFFERDI STEIYQAGSTPCNGVEGFNCYFPLQSYGFOPT 500  
6Z43(H11-D4) 410 IAPGQTGKIADYNYKLPDDFTGCVI AWNSNNLDSKVGNNYLYRLFRKSNLKPFFERDI STEIYQAGSTPCNGVEGFNCYFPLQSYGFOPT 500  
7BYR(BD23) 410 IAPGQTGKIADYNYKLPDDFTGCVI AWNSNNLDSKVGNNYLYRLFRKSNLKPFFERDI STEIYQAGSTPCNGVEGFNCYFPLQSYGFOPT 500  
3D0G(ACE2) 397 IAPGQTGVIADYNYKLPDDFMGCVLAWNTRNIDATSTGNYNYKYRRLRHGKLRPFERDI SNVPFSPDGKPCT - PPALNCYWP LNDYGFYTT 486  
2DD8(m396) 397 IAPGQTGVIADYNYKLPDDFMGCVLAWNTRNIDATSTGNYNYKYRRLRHGKLRPFERDI SNVPFSPDGKPCT - PPALNCYWP LNDYGFYTT 486  
6NB6(S230) 397 IAPGQTGVIADYNYKLPDDFMGCVLAWNTRNIDATSTGNYNYKYRRLRHGKLRPFERDI SNVPFSPDGKPCT - PPALNCYWP LNDYGFYTT 486  
6WAQ(VHH-72) 397 IAPGQTGVIADYNYKLPDDFMGCVLAWNTRNIDATSTGNYNYKYRRLRHGKLRPFERDI SNVPFSPDGKPCT - PPALNCYWP LNDYGFYTT 486  
2GHW(80R) 397 IAPGQTGVIADYNYKLPDDFMGCVLAWNTRNIDATSTGNYNYKYRRLRHGKLRPFERDI SNVPFSPDGKPCT - PPALNCYWP LNDYGFYTT 486  
3BGF(F26G19) 397 IAPGQTGVIADYNYKLPDDFMGCVLAWNTRNIDATSTGNYNYKYRRLRHGKLRPFERDI SNVPFSPDGKPCT - PPALNCYWP LNDYGFYTT 486

6M0J(ACE2) 501 NGVGYPYRVVLSFELLHAPATVCGPKKSTNLVKNKCVNF 541  
6WPS(S309) 501 NGVGYPYRVVLSFELLHAPATVCGPKKSTNLVKNKCVNF 541  
6W41(CR3022) 501 NGVGYPYRVVLSFELLHAPATVCGPKKSTNLVKNKCVNF 541  
7C01(CB7) 501 NGVGYPYRVVLSFELLHAPATVCGPKKSTNLVKNKCVNF 541  
7BWJ(P2B-2F6) 501 NGVGYPYRVVLSFELLHAPATVCGPKKSTNLVKNKCVNF 541  
7BZ5(B38) 501 NGVGYPYRVVLSFELLHAPATVCGPKKSTNLVKNKCVNF 541  
6Z43(H11-D4) 501 NGVGYPYRVVLSFELLHAPATVCGPKKSTNLVKNKCVNF 541  
7BYR(BD23) 501 NGVGYPYRVVLSFELLHAPATVCGPKKSTNLVKNKCVNF 541  
3D0G(ACE2) 487 TGIQYQPYRVVLSFELLNAPATVCGPKLSTD L IKNQCVNF 527  
2DD8(m396) 487 TGIQYQPYRVVLSFELLNAPATVCGPKLSTD L IKNQCVNF 527  
6NB6(S230) 487 TGIQYQPYRVVLSFELLNAPATVCGPKLSTD L IKNQCVNF 527  
6WAQ(VHH-72) 487 TGIQYQPYRVVLSFELLNAPATVCGPKLSTD L IKNQCVNF 527  
2GHW(80R) 487 TGIQYQPYRVVLSFELLNAPATVCGPKLSTD L IKNQCVNF 527  
3BGF(F26G19) 487 TGIQYQPYRVVLSFELLNAPATVCGPKLSTD L IKNQCVNF 527

Figure 5: Illustration of the contact positions of antibody and ACE2 epitope with SARS-CoV-2 and SARS-CoV S protein RBDs on RBD two-dimensional (2D) sequences. The proteins in the structures of 6M0J, 6WPS, 6W41, 7C01, 7BWJ, 7BZ5, 6Z43, and 7BYR are in complexes with SARS-CoV-2 S-protein while the proteins in structures 3D0G, 2DD8, 6NB6, 6WAQ, 2GHW, and 3BGF are in complexes with SARS-CoV S protein.

for SARS-CoV-2 using the TopNetTree model [74].

## 4.1 Ranking of ACE2 and antibodies

The prediction results and network descriptors are presented in Table 2 and Table 3 for SARS-CoV-2 complexes and SARS1 complexes, respectively. In Table 2, the complexes are ranked according to their predicted binding affinities,  $\Delta G$ , followed by FRI rigidity indexes [43, 83] which have the highest covariance. They are computed based on all the  $C_{\alpha}$  atoms on the RBD and all the  $C_{\alpha}$  atoms in antibodies or ACE2. The FRI rigidity index  $R_{\eta}$  indicates the measurement of geometric compactness and topological connectivity of protein-protein interactions at each residue, such that more impact of the longer pairwise interactions for larger  $\eta$ . Comparing with the predicted energy, a strong binding affinity is corresponding to a large rigidity index. Then the summation of binding affinity changes computed with the TopNetTree model [74] by modifying the RBD residues to glycine (G) are presented while  $S_{10}$  and  $S_8$  stand for those residues within 10Å and 8Å to the binding site are included. Each mutation to glycine (G) is calculated by PPI machine learning model [74], where a positive binding affinity changes  $\Delta\Delta G$  means a stronger binding affinity of mutant and vice versa. Therefore, a summation of considered residues in the RBD with smaller values indicates a strong binding affinity of wild type.

The rest of the table gives the  $C_{\alpha}$ -based complex analysis from a number of network descriptors, including edge density ( $d$ ), degree heterogeneity ( $\rho$ ) [17], average path length ( $\langle L \rangle$ ) [76], average betweenness centrality ( $\langle C_b \rangle$ ) [24], average eigencentrality ( $\langle C_e \rangle$ ) [2], average subgraph centrality ( $\langle C_s \rangle$ ) [21], and network communicability ( $\langle M \rangle$ ) [19]. Except for the degree heterogeneity which is calculated based only on

Table 2: The graph network descriptor consisting of SARS-CoV-2 Spike protein RBD and ACE2 and antibodies.  $\Delta G$ : the predicted binding affinity (kcal/mol) (the predictions are using the Prodigy web server [84]);  $R_{10}$  and  $R_8$ : FRI rigidity index with  $\eta$  of 10 and 8, respectively;  $S_{10}$  and  $S_8$ : the summation of binding affinity changes ( $\Delta\Delta G$  kcal/mol) by changing RBD residues within 10Å and 8Å to the binding site to glycine;  $d$ : edge density;  $\rho$ : degree heterogeneity;  $\langle L \rangle$ : average path length;  $\langle C_b \rangle$ : average betweenness centrality;  $\langle C_e \rangle$ : average eigencentrality;  $\langle C_s \rangle$ : average subgraph centrality;  $\langle M \rangle$ : network communicability.

Molecule	CR3022	B38	CB6	ACE2	BD23	H11-D4	S309	P2B-2F6
PDB ID	6W41	7BZ5	7C01	6M0J	7BYR	6Z43	6WPS	7BWJ
$\Delta G$	-15.4	-14.7	-13.5	-11.9	-10.8	-10.3	-9.9	-9.6
$R_{10}$	335	349	338	279	227	201	256	211
$R_8$	134	138	132	105	106	82	97	82
$S_{10}$	19.15	30.17	36.56	20.83	10.39	8.91	18.28	17.74
$S_8$	11.69	12.39	13.36	16.60	5.49	4.41	7.04	5.97
$d$	0.070	0.069	0.072	0.072	0.069	0.077	0.071	0.074
$\rho$	0.0192	0.0190	0.0196	0.0185	0.0171	0.0190	0.0206	0.0196
$\langle L \rangle$	13.69	14.26	13.75	13.85	14.80	13.59	13.86	13.98
$\langle C_b \rangle$	0.0109	0.0111	0.0110	0.0113	0.0130	0.0113	0.0112	0.0117
$\langle C_e \rangle$	0.052	0.050	0.052	0.051	0.053	0.054	0.054	0.053
$\langle C_s \rangle$	1590955	2397825	2010826	2105421	813061	2248985	1387110	1562243
$\langle M \rangle$	847509	1237464	1096771	1132331	413572	1239452	753625	855641
$\langle \Theta \rangle$	0.0192	0.0190	0.0196	0.0185	0.0171	0.0190	0.0206	0.0196

the RBD  $C_\alpha$  atoms, other descriptors are calculated from all  $C_\alpha$  atoms on the RBD and antibody (or ACE2)  $C_\alpha$  atoms within 10Å from any  $C_\alpha$  atom on the RBD. The degree heterogeneity demonstrates antibody or ACE2 influence to the RBD, such that close degree heterogeneity numbers would have similar impacts. For example, molecules B38 and H11-D4 have degree heterogeneity values that are close to ACE2 as well as sharing the same receipt domain. As for other descriptors, the average betweenness centrality [24] and average eigencentrality [2] values are correlated quite well to the predicted binding affinities.

Table 3 shows the results of predictions and network descriptors for the SARS-CoV S protein complex. Again, the predicted binding affinities have high correlations to FRI rigidity indexes. For degree heterogeneity, m396 has a similar impact as ACE2. In Table 3, molecule 80R (PDB 2GHW) has the highest rigidity index both for  $\eta = 10$  and  $\eta = 8$  which indicates a more rigid complex structure between 80R and the RBD. In the comparison of SARS-CoV S protein RBD and SARS-CoV-2 S protein RBD in Table 2, descriptors are close to each other except for the summation of binding affinity changes which includes more biological and chemical information than others. Thus, the network structures for SARS-CoV RBD and SARS-CoV-2 RBD complex are similar.

## 4.2 Prediction of binding affinity changes following mutations

In this section, we predict the binding affinities of SARS-CoV antibodies when they are applied to SARS-CoV-2 neutralization. Specifically, we compute the binding affinity changes following the mutations from SARS-CoV RBD to SARS-CoV-2 RBD. These changes can be very significant. Study shows that a single mutation (V367F) can lead to a 10-fold increase in  $IC_{50}$  for a particular antibody [54].

In Figure 6, the blue bars are predicted binding affinities of each SARS-CoV-2 complex, and the red bars are predicted binding affinities of each molecule with SARS-CoV-2 RBD, which is calculated by accumulating binding affinities of single mutations from SARS-CoV RBD to SARS-CoV-2 RBD and adding the sum to the binding affinities of SARS-CoV complexes. Obviously, molecule 80R (PDB: 2GHW) has the largest binding energy change in SARS-CoV ranking as well as in SARS-CoV-2 ranking among these SARS-CoV antibodies. Molecule VHH-72 (6WAQ) had a smaller binding affinity than ACE2(3D0G) does for SARS-CoV

Table 3: The graph network descriptor consisting of SARS-CoV Spike protein RBD and ACE2 and antibodies.  $\Delta G$ : the predicted binding affinity (kcal/mol) (the predictions are using the Prodigy web server [84]);  $R_{10}$  and  $R_8$ : FRI rigidity index with  $\eta$  of 10 and 8, respectively;  $S_{10}$  and  $S_8$ : the summation of binding affinity changes ( $\Delta\Delta G$  kcal/mol) by changing RBD residues within 10Å and 8Å to the binding site to glycine;  $d$ : edge density;  $\rho$ : degree heterogeneity;  $\langle L \rangle$ : average path length;  $\langle C_b \rangle$ : average betweenness centrality;  $\langle C_e \rangle$ : average eigencentality;  $\langle C_s \rangle$ : average subgraph centrality;  $\langle M \rangle$ : network communicability.

Molecule	80R	ACE2	VHH-72	m396	S230	F26G19
PDB ID	2GHW	3D0G	6WAQ	2DD8	6NB6	3BGF
$\Delta G$	-17.3	-11.5	-9.7	-9.4	-7.7	-6.7
$R_{10}$	378	270	255	304	195	254
$R_8$	157	101	103	119	72	101
$S_{10}$	20.35	13.05	13.37	10.79	11.48	14.01
$S_8$	8.92	1.56	7.49	6.47	8.09	7.84
$d$	0.070	0.070	0.074	0.073	0.078	0.072
$\rho$	0.0206	0.0187	0.0193	0.0186	0.0197	0.0190
$\langle L \rangle$	13.35	12.91	13.46	12.90	12.96	12.63
$\langle C_b \rangle$	0.0120	0.0108	0.0109	0.0113	0.0119	0.0113
$\langle C_e \rangle$	0.053	0.053	0.053	0.054	0.054	0.056
$\langle C_s \rangle$	2693776	1418662	1607217	2383597	3167175	1897873
$\langle M \rangle$	1446506	730809	915061	1311299	1714397	1039376
$\langle \Theta \rangle$	0.0206	0.0187	0.0192	0.0186	0.0196	0.0190

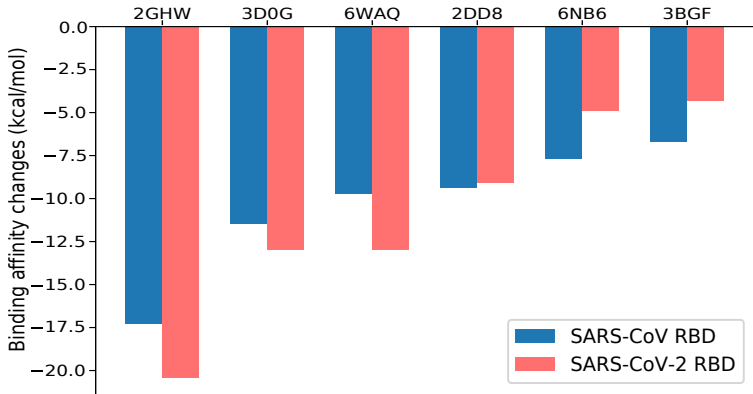


Figure 6: An illustration of the binding affinities of antibodies with SARS-CoV and SARS-CoV-2 RBD. Molecular names of these antibodies are 80R (PDB: 2GHW), ACE2 (3D0G), VHH-72 (6WAQ), m396 (2DD8), S230 (6NB6), and F26G19 (3BGF).

RBD while an equivalent binding affinity for SARS-CoV-2 RBD. Molecules m396, S230, and F26G19 have weaker binding affinities after modifying from SARS-CoV RBD to SARS-CoV-2 RBD. Finally, the binding affinity of SARS-CoV RBD with ACE2 following mutations to SARS-CoV-2 is slightly higher than the binding affinity of SARS-CoV RBD with ACE2, indicating that SARS-CoV-2 is more infectious than SARS-CoV. This is consistent with experimental reports [67, 79].

Figures 7 and 8 show the binding affinity changes on individual mutations on the SARS-CoV S protein RBD, where more precise trends can be observed. In Figure 7, molecule, 80R, has a similar trend to ACE2 which shares the most receiving domain. In Figure 8, most of the binding affinity changes following mutations in receptor binding motif (RBM) of ACE2 are negative, which indicates stronger binding affinities with SARS-CoV RBD.

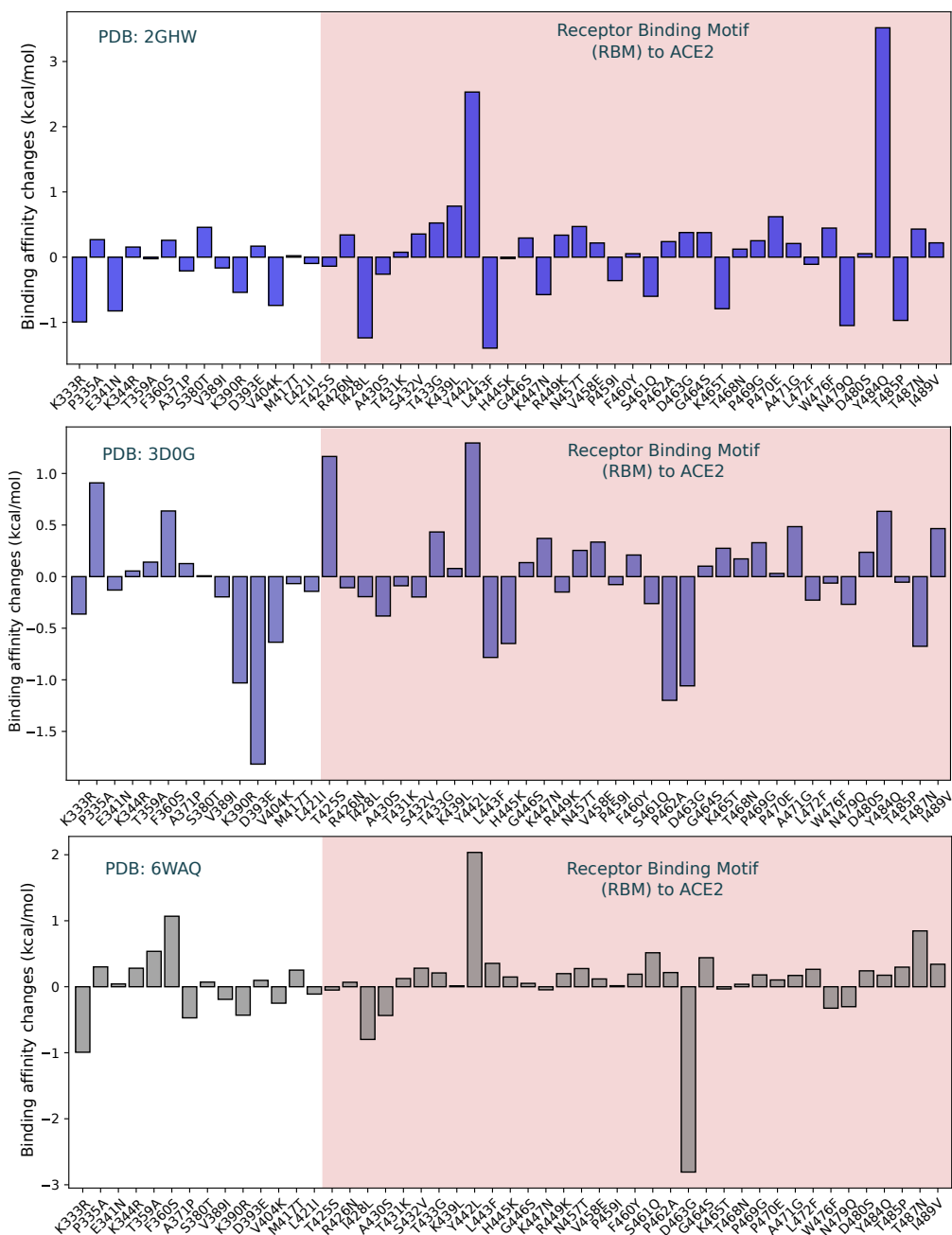


Figure 7: Overall binding affinity changes on the S protein receptor-binding domain (RBD) from SARS-CoV to SARS-CoV-2 of molecules 80R, ACE2, and VHH-72. The x-axis records the wild type to the mutate type at the specific residue position. The pink color region marks the receptor-binding motif (RBM) corresponding to ACE2. The height of each bar indicates the predicted binding affinity changes. A positive change indicates a strengthening in binding.

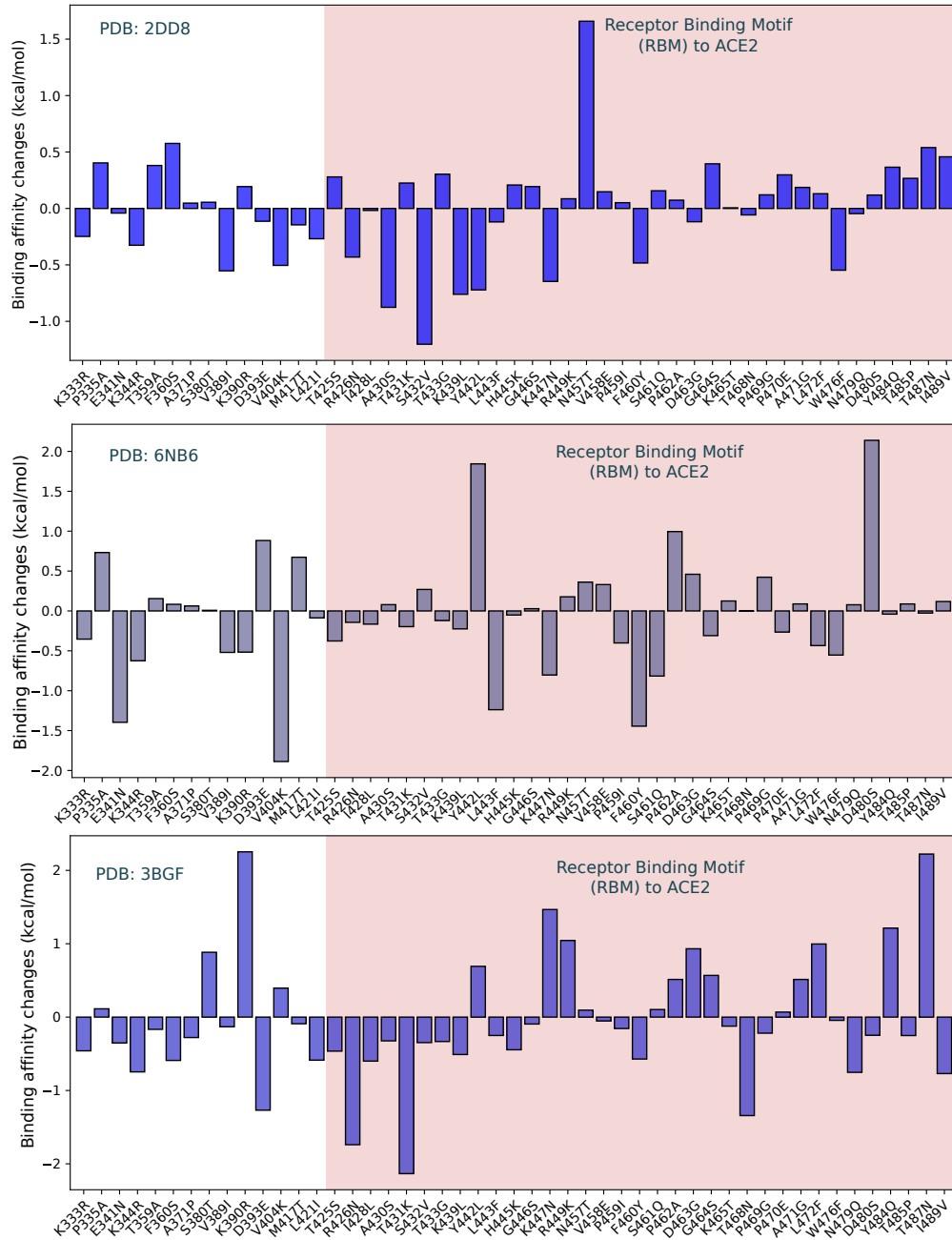


Figure 8: Overall binding affinity changes on the S protein receptor-binding domain (RBD) from SARS-CoV to SARS-CoV-2 of molecules m396, S320, and F26G19. The x-axis records the wild type to the mutate type at the specific residue position. The pink color region marks the receptor-binding motif (RBM) corresponding to ACE2. The height of each bar indicates the predicted binding affinity changes. A positive change indicates a strengthening in binding.

### 4.3 Network analysis of antibody-antigen complexes

Various network models have been employed to analyze the structure and function of SARS-CoV and SARS-CoV-2 main protease [18]. In this work, we utilize network models to illustrate interactions between the binding complexes of the RBD of SARS-CoV or SARS-CoV-2 and antibodies or ACE2.

In the microscopy of each single residue, their performances on network models reveal the similarities and differences between complexes. In Figure 9, SARS-CoV RBD with ACE2 (PDB: 3D0G), SARS-CoV-2 RBD with ACE2 (PDB: 6M0J), and SARS-CoV-2 RBD with CR3022 (PDB: 6W41) are listed and aligned where 6W41 has the strongest predicted binding affinity and the largest deviation to 6M0J as shown in Tables 2 and 3. The  $C_{\alpha}$  atoms from the RBD are marked as a circle, and atoms from ACE2 or CR3022 are marked as a cube. In the first row of Figure 9, it is interesting to observe all three complexes having similar domains that have high rigidity index values. In the comparison of betweenness centralities of three structures, though it is shown clearly that 3D0G has many large values, it has the lowest average betweenness centrality among the structures as shown in Tables 2 and 3. Analogy to the rigidity index, all three complexes have the same regions of the individual eigencentality values and subgraph centrality values. Overall, the differences between 3D0G and 6M0J are quite close in their network analysis. However, the betweenness centrality reflects their difference such that a higher average value would indicate a stronger binding affinity. Moreover, all three complexes coincidentally have similar regions of high values for network descriptors, which suggests that this region would play a key role in protein-protein interactions.

## 5 Clinical trials of COVID-19 antibody therapeutic candidates

Table 4 summarizes the currently ongoing clinical trials of COVID-19 antibody therapeutic candidates in the United States, China and Europe. These data are collected from the National Institutes of Health (NIH) (<https://www.nih.gov/coronavirus>), the European Medicines Agency (EMA) (<https://www.clinicaltrialsregister.eu/ctr-search/search?query=covid-19>), and the media's reports.

Notably, most of the current COVID-19 antibody therapeutic candidates in clinical trials are aimed at other targets rather than the S protein. These antibodies were developed for other diseases initially and now repurposed to treat COVID-19, which could alleviate some COVID-19 symptoms such as cytokine storm and inflammation instead of killing the viruses.

Nonetheless, two antibody candidates under clinical trials are targeting at S protein and block the SARS-CoV-2 entry into human cells. One is LY3819253 developed by Eli Lilly and Company in the United States, which is in phase II clinical trial and already highlighted in TheScientist (<https://www.the-scientist.com/news-opinion/first-antibody-trial-launched-in-covid-19-patients--67604>). The other is JS016 performed by Junshi Biosciences in China [58], which is currently in phase I clinical trial.

Table 4: The summary of current on-going clinical trials of Covid-19 antibody therapeutic candidates.

Antibody ID	Manufacturer	Target	Trial location	Trial phase	Start date
Lanadelumab <sup>a</sup>	Shire	pKal	Radboud University Medical Center, Nijmegen, Netherlands	4	/
Octagam <sup>a</sup>	Pfizer	Antibody mixture	Sharp Memorial Hospital, San Diego, California, United States	4	4.28.2020

Sarilumab <sup>a,b</sup>	Regeneron Pharmaceuticals and Sanofi	IL-6	Assistance Publique - Hpitaux de Paris, Paris, France;	3	3.25.2020
			VA Boston Healthcare System, Boston, Massachusetts, United States	2	4.10.2020
Sirukumab <sup>a,b</sup>	Janssen Biotech	IL-6	Sanofi-aventis Recherche et Dveloppement, Chilly-Mazarin, France;	3	3.26.2020
			Loyola University Medical Center, Maywood, Illinois, United States	2	4.24.2020
Canakinumab <sup>a,b</sup>	Novartis	Interleukin-1 $\beta$	Novartis Investigative Site, Glendale, California, United States;	3	4.30.2020
			Novartis Pharma GmbH, Nrnberg, Germany	3	4.29.2020
IFX-1 <sup>b</sup>	InflaRx	C5a	InflaRx GmbH, Jena, Germany	3	3.29.2020
Lenzilumab <sup>a</sup>	Humanigen	GM-CSF	Mayo Clinic, Phoenix, Arizona, United States	3	4.30.2020
Mylotarg <sup>b</sup>	Celltech and Wyeth	CD33	UK Research and Innovation, United Kingdom	3	5.5.2020
Ravulizumab <sup>b</sup>	Alexion Pharmaceuticals	C5	Alexion Europe SAS, Levallois-Perret, France	3	5.7.2020
Tocilizumab <sup>a,b</sup>	Roche	IL-6	Queen's Medical Center, Honolulu, Hawaii, United States;	3	6.1.2020
			F. Hoffmann-La Roche Ltd, Basel, Switzerland	3	4.6.2020
Avdoralimab <sup>b</sup>	Innate Pharma	C5a	Assistance Publique Hopitaux De Marseille, Marseille, France	2	4.23.2020
Bevacizumab <sup>b</sup>	Genentech	VEGF-A	Fundacin para la Investigacin Biomdica de Crdoba, Crdoba, Spain	2	4.24.2020
CERC 002 <sup>a</sup>	Cerecor	LIGHT	Cape Fear Valley Medical Center, Fayetteville, North Carolina, United States	2	6.9.2020
Clazakizumab <sup>a</sup>	Bristol Myers Squibb and Alder Biopharmaceuticals	IL-6	Cedars-Sinai Medical Center, Los Angeles, California, United States	2	4.24.2020



Gimsilumab <sup>a</sup>	Eisai Inc	GM-CSF	UCLA Ronald Reagan Medical Center, Los Angeles, California, United States	2	4.12.2020
IC14 <sup>a</sup>	Scripps Research	CD14	University of Washington, Seattle, Washington, United States	2	7.2020
Infliximab <sup>a</sup>	Janssen Biotech	TNF $\alpha$	Tufts Medical Center, Boston, Massachusetts, United States	2	6.1.2020
Leronlimab <sup>a</sup>	CytoDyn	CCR5	University of California, Los Angeles, California, United States	2	4.1.2020
LY3127804 <sup>a</sup>	Eli Lilly and Company	Ang2	NorthShore University HealthSystem, Evanston, Illinois, United States	2	4.20.2020
LY3819253 <sup>a</sup>	Eli Lilly and Company	S protein	Cedars Sinai Medical Center, Los Angeles, California, United States	2	6.13.2020
Mavrilimumab <sup>a</sup>	MedImmune	GM-CSF	Cleveland Clinic Health System, Cleveland, Ohio, United States	2	5.20.2020
MSTT1041A <sup>a</sup>	Genentech	ST2	eStudySite-Chula Vista-PPDS, Chula Vista, California, United States	2	6.2.2020
Nivolumab <sup>b</sup>	Bristol-Myers Squibb	PD-1	Centre Lon Brard, Lon, France	2	4.1.2020
Otilimab <sup>a,b</sup>	MorphoSys	GM-CSF	GSK Investigational Site, Saint Louis Park, Minnesota, United States; GlaxoSmithKline Research Development Limited, Brentford, United Kingdom	2 2	5.28.2020 5.20,2020
Siltuximab <sup>b</sup>	Eusapharma	IL-6	Fundaci Clnic per a la Recerca Biomedica, Barcelona, Spain	2	4.7.2020
SNDX-6352 <sup>a</sup>	Syndax Pharmaceuticals	CSF-1R	HonorHealth, Scottsdale, Arizona, United States	2	5.30.2020
ARGX-117 <sup>b</sup>	Argenx	C2	Argenx BV, Zwijnaarde, Belgium	1	4.21.2020
TJ003234 <sup>a</sup>	/	GM-CSF	GW Medical Faculty Associates, Washington, District of Columbia, United States	1	4.11.2020

JS016 <sup>c</sup>	Junshi Biosciences	S protein	Huashan Hospital Affiliated to Fudan University, Shanghai, China	1	6.7.2020
--------------------	--------------------	-----------	---	---	----------

## 6 Material and methods

### 6.1 Sequences and structures

All the sequences and 3D structures are downloaded from Protein Data Bank (<https://www.rcsb.org>): the sequences are from the FASTA files, the 3D structures are from the pdb files.

The 3D alignments as well as the graphs are created by using PyMOL [13]. The 2D sequence alignment are calculated by clustalw (<https://www.genome.jp/tools-bin/clustalw>) [61], the 2D alignment graphs are generated by Jalview [75].

### 6.2 TopNetTree model for protein-protein interaction (PPI) binding affinity changes upon mutation

In this section, the topology-based network tree (TopNetTree) is presented, which predicts binding affinity changes following mutation  $\Delta\Delta G$  for PPIs [74]. This method is based on structures regarded as topological features and supervised machine learning model, gradient boosting tree (GBT), and convolution neural network (CNN). In Fig. 10, the train and predicting process is elucidated that two major modules are applied the topology-based feature generation and a CNN-assisted GBT model. In feature generation, the element- and site-specific persistent homology is the key mathematical technique that can simplify the structural complexity of protein-protein complexes and translate the biological information into topological invariants. The first step of the TopNetTree process uses CNN as an assistant model to manipulate the topological features. Assembling CNN-pretrained features and other features, the last step of the GBT model predicts PPIs binding affinity changes. Other features such as chemical and physical information that have not been absorbed into topological features can improve the proposed model's predicting ability. More details are referred to in the literature [74].

#### 6.2.1 Topology-based feature generation of PPIs

Persistence homology is the key mathematical theory behind the topology-based feature generation. As a subtopic of algebraic topology, persistence homology is built upon simplicial complex and filtration on discrete datasets under various settings. For example, the set of atoms in protein-protein interactions forms the discrete dataset. When building the constructions, a variety of simplicial complex built on point clouds such that Vietoris-Rips (VR) complex and alpha complex are widely used [16] which are applied in our

<sup>2</sup>List of links of antibodies in Table 4:

<sup>a</sup> <https://clinicaltrials.gov/ct2/results?recrs=ab&cond=covid-19&term=&cntry=US&state=&city=&dist=>

<sup>b</sup> <https://www.clinicaltrialsregister.eu/ctr-search/search?query=covid-19>

<sup>c</sup> <https://www.globenewswire.com/news-release/2020/06/07/2044620/0/en/Junshi-Biosciences-Announces-Dosing-of-First-Healthy-Volunteer-in-Phase-I-Clinical-Study-of-SARS-CoV-2-Neutralizing-Antibody-JS016-in-China.html>

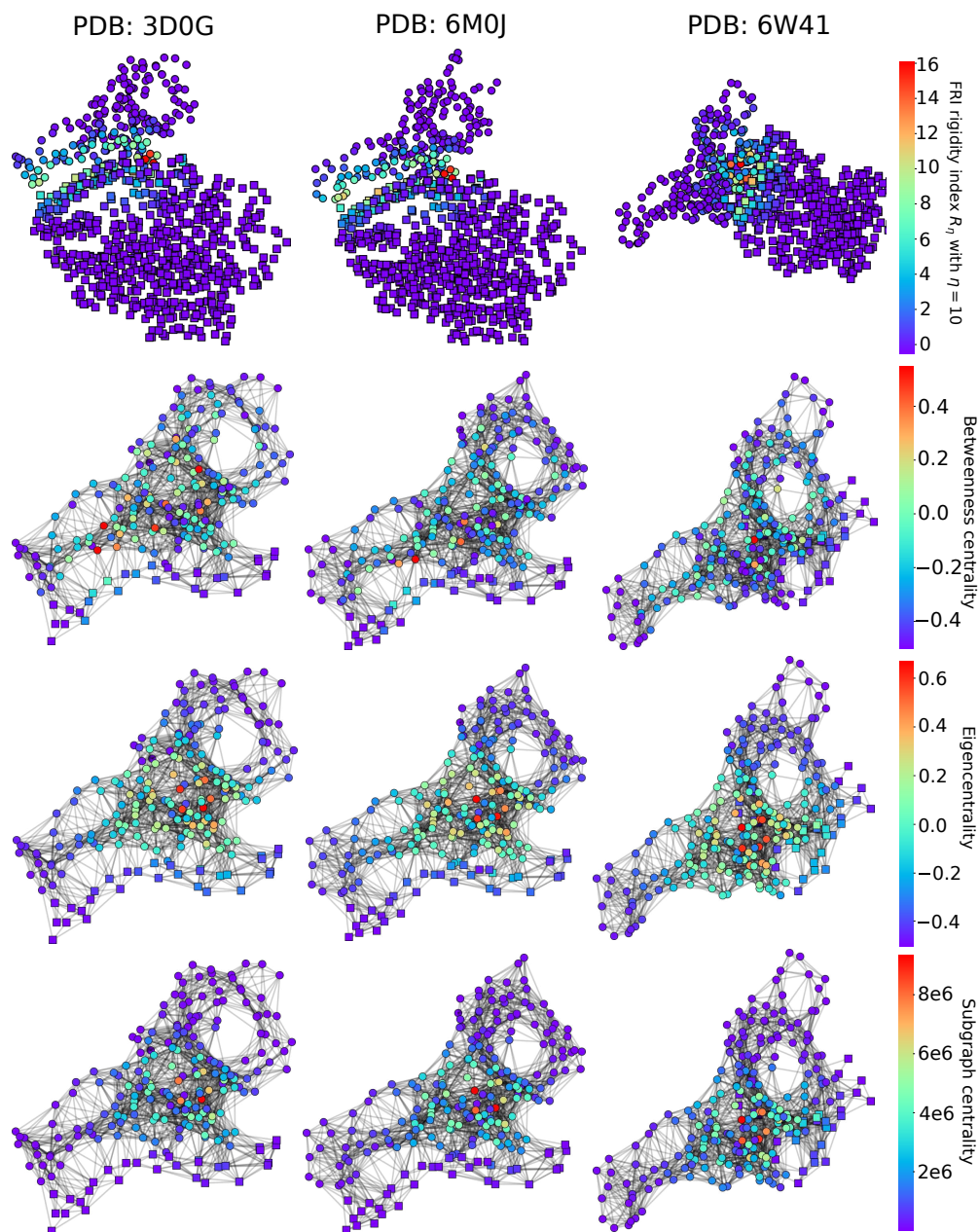


Figure 9:  $C_\alpha$  network analysis of three antibody-antigen complexes. Circle markers are for antigen (spike protein RBD) and cube markers are for antibody or ACE2. Columns list complexes 3D0G, 6M0J, and 6W41. Rows represent FRI rigidity index, betweenness centrality, eigencentrality, and subgraph centrality.

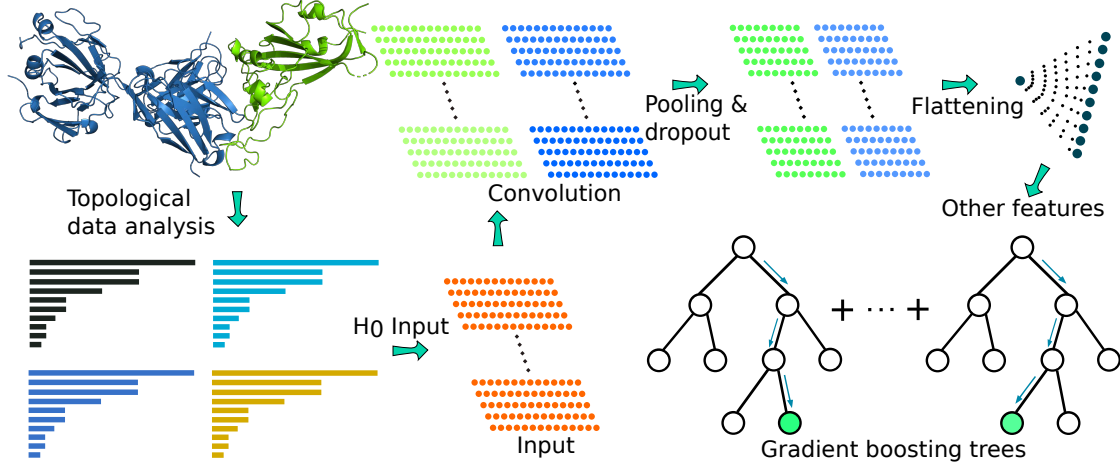


Figure 10: An illustration of the TopNetTree model [74]. Protein structure shown in the plot is SARS-CoV-2 spike receptor-binding domain bound with antibody (PDB 7BZ5). Here,  $H_0$  are the 0-dimensional topological input features for machine learning model.

approach. After a simplicial complex set up, the topological invariants of the point-cloud dataset can be identified and are enumerated by counting the numbers referred to as Betti-0 ( $H_0$ ), Betti-1 ( $H_1$ ), and Betti-2 ( $H_2$ ) for components, rings, and cavities of dataset, respectively. Obviously, the complexity protein-protein structure is simplified as its geometric and topological characteristics for data features, while redundant and uninformative features or calculations are fully abandoned. Moreover, making filtration on simplicial complex turns the 3D point-cloud dataset of PPIs into topological barcodes, which record the “birth” and “death” of each topological invariants. The topological features simplify the PPI-complex in many directions. However, it is also essential to have better construction to reflect different biological or chemical properties. Various subsets are defined as following for PPI complex constructions.

1.  $\mathcal{A}_m$ : atoms of the mutation sites.
2.  $\mathcal{A}_{mn}(r)$ : atoms in the neighbourhood of the mutation site within a cut-off distance  $r$ .
3.  $\mathcal{A}_{Ab}(r)$ : antibody atoms within  $r$  of the binding site.
4.  $\mathcal{A}_{Ag}(r)$ : antigen atoms within  $r$  of the binding site.
5.  $\mathcal{A}_{ele}(E)$ : atoms in the system that has atoms of element type  $E$ .

Therefore, the distance matrix is defined based on atom sets such that it excludes the interactions in the same set. For interactions between atoms  $a_i$  and  $a_j$  in set  $\mathcal{A}$  and/or set  $\mathcal{B}$ , the modified distance is defined as

$$D_{\text{mod}}(a_i, a_j) = \begin{cases} \infty, & \text{if } a_i, a_j \in \mathcal{A}, \text{ or } a_i, a_j \in \mathcal{B}, \\ D_e(a_i, a_j), & \text{if } a_i \in \mathcal{A} \text{ and } a_j \in \mathcal{B}, \end{cases} \quad (1)$$

where  $D_e(a_i, a_j)$  is the Euclidian distance between  $a_i$  and  $a_j$ . Next, the persistence homology can be constructed element- and site-specific.

Given atomic coordinates, their topological analysis and properties can be carried out via simplices and simplicial complexes. A set of  $k+1$  affinely independent points,  $v_0, v_1, v_2, \dots, v_k$  in  $\mathbb{R}^n$  is a  $k$ -simplex denoted  $\sigma_i$ , such that a 0-, 1-, 2-, or 3-simplex in geometry representation is a vertex, an edge, a triangle, or a tetrahedron, respectively. The finite collection of simplex is a simplicial complex  $K = \{\sigma_i\}$ , which is true if a subset (also called as face)  $\tau$  of a  $k$ -simplex  $\sigma_i$  of  $K$  is also in  $K$ ,  $\tau \subseteq \sigma_i$  and  $\sigma_i \in K$  imply  $\tau \in K$  and the non-empty intersection of any two simplices in  $K$  is a face of both. Furthermore, a  $k$ -chain is a finite formal sum of all simplices in  $K$ ,  $\sum_i \alpha_i \sigma_i^k$ , where  $\alpha_i$  is coefficients in  $\mathbb{Z}_p$  and  $p$  is a chosen prime number. The set of all  $k$ -chains of the simplicial complex  $K$  equipped with an algebraic field forms an abelian group  $C_k(K, \mathbb{Z}_p)$ .

A boundary operator  $\partial_k : C_k \rightarrow C_{k-1}$  for a  $k$ -simplex  $\sigma^k$  is homomorphism defined as

$$\partial_k \sigma^k = \sum_{i=0}^k (-1)^i \{v_0, v_1, \dots, \hat{v}_i, \dots, v_k\},$$

where  $\{v_0, v_1, \dots, \hat{v}_i, \dots, v_k\}$  is a  $(k-1)$ -simplex excluding  $v_i$  from the vertex set. An important property of boundary operator,  $\partial_{k-1} \partial_k = \emptyset$ , follows from that boundaries are boundaryless. Moreover the kernel of boundary operator is  $Z_k = \ker \partial_k = \{c \in C_k \mid \partial_k c = \emptyset\}$ , whose elements are called  $k$ -cycles; and the  $k$ th boundary group is the image of  $\partial_{k+1}$  denoted as  $B_k = \text{im } \partial_{k+1} = \{\partial_{k+1} c \mid c \in C_{k+1}\}$ . The algebraic construction to connect a sequence of complexes by boundary maps is called a chain complex

$$\dots \xrightarrow{\partial_{i+1}} C_i(X) \xrightarrow{\partial_i} C_{i-1}(X) \xrightarrow{\partial_{i-1}} \dots \xrightarrow{\partial_2} C_1(X) \xrightarrow{\partial_1} C_0(X) \xrightarrow{\partial_0} 0$$

and the  $k$ th homology group is the quotient group defined by  $H_k = Z_k / B_k$ . Obviously, boundary operators imply  $B_k \subseteq Z_k \subseteq C_k$ . The Betti numbers are defined by the number of basis in  $k$ th homology group  $H_k$  which counts  $k$ -dimensional holes. For example, Betti 0,  $\beta_0 = \text{rank}(H_0)$  reflects the number of connected components; Betti 1,  $\beta_1 = \text{rank}(H_1)$  reflects the number of loops; and Betti 2,  $\beta_2 = \text{rank}(H_2)$  reveals the number of voids or cavities. Together, the set of Betti numbers  $\{\beta_0, \beta_1, \beta_2, \dots\}$  indicates the intrinsic topological property of a system. Computational, boundary operators directly work on the distance matrices generated on different atom groups, and the Betti number can be calculated by counting the number of zero eigenvalues of corresponding boundary operators.

It is interested in the evolution of a simplicial complex and to track topological characteristics varying as the simplicial complex changes. In persistent homology, a filtration of a topology space  $K$  is a nested sequence of subspaces  $\{K^t\}_{t=0, \dots, m}$  of  $K$  such that  $\emptyset = K^0 \subseteq K^1 \subseteq K^2 \subseteq \dots \subseteq K^m = K$ . Considering the complex group on this sequence, we can have a sequence of chain complexes by homomorphisms:  $C_*(K^0) \rightarrow C_*(K^1) \rightarrow \dots \rightarrow C_*(K^m)$  and a corresponding homology sequence:  $H_*(K^0) \rightarrow H_*(K^1) \rightarrow \dots \rightarrow H_*(K^m)$ . The  $p$ -persistent  $k$ th homology group of  $K^t$  is defined as  $H_k^{t,p} = Z_k^t / (B_k^{t+p} \cap Z_k^t)$ , where  $B_k^{t+p} = \text{im } \partial_{k+1}(K^{t+p})$ . Hence, the homology group reveals that the homology classes of  $K^t$  persist until  $K^{t+p}$ . In the filtration process, the persistent homology barcodes recording the ‘‘birth’’ and ‘‘death’’ of topological invariants can be generated along the spacial changing of radius on point-cloud dataset. The machine learning feature vectors, as consequences, can be constructed from theses sets of filtration barcode intervals.

The filtration parameter interval is discretized into bins, which can model the behavior of barcodes in each bin [5]. Thus, these bins are packaged as features for advanced machine learning algorithms directly. Then the number of persistence intervals is counted for each bin in order to record birth events and death events. Three feature vectors ( $H_0$ ,  $H_1$ , and  $H_2$ ) are generated for each topological barcode for the machine learning method. Betti-0 ( $H_0$ ) barcode is obtained from the VR filtration and Betti-1 ( $H_1$ ), and Betti-2 ( $H_2$ ) barcode is obtained from alpha complex filtration, where Betti-1 and Betti-2 are sparser and more stable than Betti-0 barcodes. Thus, Betti-0 barcode is incorporated into CNN models, and Betti-1 and Betti-2 barcodes are for GBT training. Intuitively, features generated by binned barcode vectorization can reflect the structure of the protein-protein complex and its biological and chemical properties, such as the strength of atom bonds, van der Waals interactions. Meanwhile, taking the statistics of bar lengths, birth values, and death values, such as maximum, minimum, mean, etc., can be set as features for the machine learning process.

## 6.2.2 Machine learning models

To predict the binding affinity changes following mutations for PPIs is very challenging due to the complex dataset and different 3D structures. To overcome this challenge, a hybrid machine learning algorithm

which integrates a CNN and GBT to predict the binding affinity changes. The vectorized  $H_0$  barcode feature is converted into concise features by the CNN method. Then combine CNN-trained features and the rest features as the full feature set to train a GBT module for a robust predictor with effective control of overfitting.

CNN is considered as the most successful architectures as a class of deep neural networks. CNN is a regularized case of a multilayer connected neural network. Each neuron is connected locally to the next convolution layer neurons, and the weights are shared in different locations. In TopNetTree, CNN is an intermediate model that applies vectorized  $H_0$  features into a higher-level abstract feature for the gradient boosting tree method. Next, the GBT is an ensemble method that builds a powerful module for regression and classification problems as weak learners. The method sums the weak learners to eliminate the overall error based on the assumption that each learner is likely to make different mistakes. According to the current prediction error on the training dataset, the ensemble method is built upon a decision tree structure. GBT with topological features (TopGBT) is relatively robust against hyperparameter tuning and overfitting, and is suitable for a moderate number of features. The current work uses the GBT package provided by scikit-learn (v 0.23.0) [46].

Finally, TopNetTree follows the process (Fig. 10) that a supervised CNN model is trained for extracting high-level features from  $H_0$  barcodes, where the PPI  $\Delta\Delta G$  is a label. Then the flatten layer neural outputs of CNN are ranked as their importance in a GBT model. Based on the importance, the whole features consist of an ordered subset of CNN-trained features, high-dimensional topological barcodes,  $H_1$  and  $H_2$ , and auxiliary features for the final GBT model. As for the parameters, an optimal parameter setting with the best result of the 10-fold evaluation is selected from the experiments of different parameter settings.

### 6.2.3 Cross-validation of TopNetTree

Table 5: Ten-fold cross-validation of the TopNetTree on the SKEMPI 2.0 dataset.

	$R_p$	$\tau$	RMSE (kcal/mol)		$R_p$	$\tau$	RMSE (kcal/mol)
Fold 1 (Train)	0.981	0.884	0.366	Fold 6 (Train)	0.983	0.904	0.353
Fold 1 (Test)	0.835	0.595	1.065	Fold 6 (Test)	0.836	0.594	1.064
Fold 2 (Train)	0.982	0.902	0.360	Fold 7 (Train)	0.983	0.904	0.356
Fold 2 (Test)	0.839	0.600	1.061	Fold 7 (Test)	0.838	0.594	1.060
Fold 3 (Train)	0.982	0.887	0.366	Fold 8 (Train)	0.979	0.878	0.392
Fold 3 (Test)	0.837	0.595	1.068	Fold 8 (Test)	0.840	0.596	1.061
Fold 4 (Train)	0.981	0.880	0.369	Fold 9 (Train)	0.982	0.902	0.362
Fold 4 (Test)	0.841	0.596	1.059	Fold 9 (Test)	0.838	0.596	1.069
Fold 5 (Train)	0.982	0.906	0.365	Fold 10 (Train)	0.982	0.886	0.367
Fold 5 (Test)	0.839	0.594	1.062	Fold 10 (Test)	0.835	0.596	1.064
Average (Train)	0.982	0.893	0.366				
Average (Test)	0.838	0.596	1.063				

The proposed TopNetTree method is trained on the SKEMPI 2.0 dataset [33], which has 4,169 variants in 319 different complexes. A set "S8338" with 8,338 variants was derived from SKEMPI 2.0 dataset by setting the reverse mutation energy changes to the negative values of its original energy changes. To address the reliability of the TopNetTree method, we did the tenfold cross-validation on the SKEMPI 2.0 dataset with the averaged training accuracy, Pearson correlation coefficients  $R_p$ , Kendall's  $\tau$ , and the root mean square error (RMSE), being 0.98, 0.89, and 0.37 kcal/mol. As shown in Table 5, these metrics are based on the

average of ten ten-fold cross-validations, which indicate TopNetTree is well trained. The performance test of tenfold cross-validation on dataset gives as  $R_p = 0.84$ ,  $\tau = 0.60$ , and  $RMSE = 1.06$  kcal/mol, which is of the same level of accuracy as the best in the literature [74].

### 6.3 Graph network analysis

Graph networks represent interactions between pairs of units in biomolecular systems. The quantify unique characteristics of the networks can be measured for descriptions and comparisons of different networks. Considering the protein-protein interactions as networks, each descriptor evaluates the network properties and measures how proteins connect. For instance, a fixed domain of spike protein RBD and antibodies forms a network, where residues from 320 to 518 on SARS-CoV and residue from 329 to 530 on SARS-CoV-2 are considered in terms of  $C_\alpha$  atoms. As aforementioned interaction subsets or similar subsets are defined for  $C_\alpha$  of each amino acid as following.

1.  $\mathcal{C}_{Ab}(r)$ : antibody  $C_\alpha$  atoms within  $r$  Å of the binding site, where  $r = \infty$  is for all  $C_\alpha$  atoms on antibody.
2.  $\mathcal{C}_{Ag}(r)$ : antigen  $C_\alpha$  atoms within  $r$  Å of the binding site, where  $r = \infty$  is for all  $C_\alpha$  atoms on antigen.

With these definitions, network descriptors are defined below.

**FRI rigidity index** The FRI rigidity index is a great tool to illustrate the elasticity between atoms for molecular interaction prediction [43, 83]. The molecular rigidity index is defined as a summation of all the atomic rigidity index  $\mu_{\eta,i}$  as

$$R_\eta = \sum_{i=1}^{N_{AB}} \mu_{\eta,i} = \sum_{i=1}^{N_{AB}} \sum_{j=1}^{N_{AG}} e^{-\left(\frac{\|\mathbf{r}_i - \mathbf{r}_j\|}{\eta}\right)^2}, \quad (2)$$

where  $\mathbf{r}_i$  are atom positions,  $N_{AB}$  and  $N_{AG}$  are the numbers of atoms of antibody and antigen, respectively, and  $r = \infty$  for all  $C_\alpha$  atoms such that  $\mathcal{C}_{Ab}(\infty)$  and  $\mathcal{C}_{Ag}(\infty)$ . The molecular rigidity index is used to describe the behavior of the dynamics and elastostatics of the biomolecular elasticity where  $\eta$  controls the influence range between atoms. In PPIs, the elasticity between antibody and antigen, especially long range impacts, is studied by calculating the FRI index of the network consisting of  $C_\alpha$  atoms.

**Degree heterogeneity** The degree heterogeneity is an index that evaluates the heterogeneity of a network on different distribution [17]. The degree distribution  $k_i$  is the number of  $i$ -th nodes that have  $k_i$  connections to other nodes. Therefore, the degree heterogeneity reflects the distributions of a network on different impacts, which is defined as

$$\rho = \sum_{i=1}^{N_e} \sum_{j=i+1}^{N_e} (k_i^{-1/2} - k_j^{-1/2})^2. \quad (3)$$

Here,  $N_e$  represents for the number of edges. In our case, we study two networks consisting of all  $C_\alpha$  atoms in  $\mathcal{C}_{Ag}(\infty)$ , that one network consists of  $C_\alpha$  atoms from SARS-CoV RBD and SARS-CoV-2 RBD. The degree heterogeneity illustrate the impacts of ACE2 or antibodies to these networks.

The rest descriptors are build on the network consist of  $C_\alpha$  atoms from  $\mathcal{C}_{Ag}(\infty)$  and  $\mathcal{C}_{Ab}(10)$ .

**Edge density** The edge density is defined as

$$d = \frac{2N_e}{N_v(N_v - 1)}, \quad (4)$$

where  $N_e$  is the number of edges and  $N_v$  is the number of vertices for  $C_\alpha$  atoms from  $\mathcal{C}_{Ag}(\infty)$  and  $\mathcal{C}_{Ab}(10)$ . The edge density is also called the average degree centrality. For a complete network in which each every pair of network vertices is connected, the edge density is equal to one. A non-complete network has an edge



density smaller than one. With the same number of residues in RBD for each PPI, a higher edge density stands for a firmly connection between RBD and ACE2 or antibodies.

**Average path length** The characteristic path length studies the typical separation between two vertices in the network. It was used to study infectious diseases spread in so called “small-world” networks [76]. The shortest path distance  $d(i, j)$  is defined as the shortest path between the corresponding pairs of vertex  $i$  and  $j$ . In protein-protein interactions, the path length between two atoms reflects how ACE2 or antibodies connect to RBD. The average path length is defined as

$$\langle L \rangle = \frac{1}{N_v(N_v - 1)} \sum_{i=1}^{N_v} \sum_{j=i+1}^{N_v} d(i, j), \quad (5)$$

for  $C_\alpha$  atoms from  $\mathcal{C}_{Ag}(\infty)$  and  $\mathcal{C}_{Ab}(10)$ . Here,  $N_v$  represents for the number of vertices.

**Average betweenness centrality** The concept of betweenness centrality illustrates communications in a network [24]. The betweenness centrality of a vertex  $v_k$  is given as

$$C_b(v_k) = \sum_{i=1}^{N_v} \sum_{j=i+1}^{N_v} g_{ij}(v_k) / g_{ij} \quad (6)$$

and the average betweenness centrality is given as

$$\langle C_b \rangle = \frac{1}{N_v} \sum_{k=1}^{N_v} C_b(v_k), \quad (7)$$

where  $g_{ij}(v_k)$  is defined as the number of geodesics linking between vertex  $v_i$  and  $v_j$  that passes  $v_k$ , and  $g_{ij}$  considers all the paths between  $v_i$  and  $v_j$ . And  $N_v$  means the number of vertices.

**Average eigencentality** The eigenvector centrality are the elements of the eigenvector  $V_{\max}$  with respect to the largest eigenvalue of the adjacency matrix  $A$  [2]. It describes the probability of starting and returning at the same point for infinite length walks. Thus the average eigenvector centrality is,

$$\langle C_e \rangle = \frac{1}{N_v} \sum_{i=1}^{N_v} e_i, \quad (8)$$

where  $e_i$  are elements of  $V_{\max}$ . It stands for the average impact spread of vertices beyond its neighborhood for an infinite walk.

**Average subgraph centrality** The following descriptors are built on the exponential of the adjacency matrix,  $E = e^A$ . The average subgraph centrality is defined as

$$\langle C_s \rangle = \frac{1}{N_v} \sum_{k=1}^{N_v} E(k, k), \quad (9)$$

which indicates the vertex participating in all subgraphs of the graphs [18, 21]. Here,  $E(k, k)$  means the element located at the  $k$ -th row and  $k$ -th column. Subgraph centrality is the summation of weighted closed walks of all lengths starting and ending at same node. The long path length has a small contribution.

**Average communicability** Finally, the last two descriptors are average communicability given as

$$\langle M \rangle = \frac{2}{N_v(N_v - 1)} \sum_{i=1}^{N_v} \sum_{j=i+1}^{N_v} E(i, j), \quad (10)$$

and average communicability angle given as

$$\langle \Theta \rangle = \frac{2}{N_v(N_v - 1)} \sum_{i=1}^{N_v} \sum_{j=i+1}^{N_v} \theta(i, j), \quad (11)$$

where  $\theta(i, j) = \arccos\left(\frac{E(i, j)}{\sqrt{E(i, i)E(j, j)}}\right)$  and  $E$  is the exponential of the adjacency matrix. The average communicability measures how much two vertices can communicate by using all the possible paths in the network, where the shorter path has more weight [19]. The average communicability angle evaluates the efficiency of two vertices passing impacts to each other in the network with all possible paths [18, 20].

## Conclusion

Currently, developing effective therapies for combating Coronavirus disease 2019 (COVID-19) caused by severe acute respiratory syndrome coronavirus 2 (SARS-CoV-2) becomes a vital task for human health and the world economy. Although designing new anti-SARS-CoV-2 drugs is of paramount importance, traditional drug discovery might take many years. Effective vaccines typically require more than a year to develop. Therefore, a more efficient strategy in fighting against COVID-19 is to look for antibody therapies, which is a relatively easier technique compared to the development of small-molecular drugs or vaccines. Seeking possible antibody drugs has attracted increasing attention in recent months. Moreover, complementarity determining regions (CDRs) which located in the tip of the antibody, determine the specificity of antibodies and make the antibody therapies a promising way to fight against COVID-19. We analyze the structure, function, and therapeutic potential of seven SARS-CoV-2 neutralizing antibody candidates that have three-dimensional (3D) structures available in the Protein Data Bank. In a comparative study, we also review five antibody structures associated with SARS-CoV and angiotensin-converting enzyme 2 (ACE2) complexes with both SARS-CoV-2 and SARS-CoV spike proteins. The multiple order of magnitude discrepancies in reported experimental binding affinities motivates us to carry a systematic computational analysis of the aforementioned fourteen complexes. Using computational topology, machine learning, and wide class network models, we put all of the complexes in an equal footing to evaluate binding and interactions. Additionally, we have predicted binding affinities of five SARS-CoV antibodies when they are used as SARS-CoV-2 therapies. Finally, we summarize all of the currently ongoing clinical antibody trails for SARS-CoV-2, which have many targets, including the S protein. In a nutshell, we provide a review of existing antibody therapies for COVID-19 and introduce many theoretical models to rank the potency and analyze the properties of antibodies.

## Supporting Material

Supporting Materials are available for S1: Network analysis of antibody-antigen complexes and S2: Binding affinity changes following mutations.

## Acknowledgment

This work was supported in part by NIH grant GM126189, NSF Grants DMS-1721024, DMS-1761320, and IIS1900473, Michigan Economic Development Corporation, Bristol-Myers Squibb, and Pfizer. The authors thank The IBM TJ Watson Research Center, The COVID-19 High Performance Computing Consortium, NVIDIA, and MSU HPCC for computational assistance.

## References

- [1] J. S. Blum, P. A. Wearsch, and P. Cresswell. Pathways of antigen processing. *Annual review of immunology*, 31:443–473, 2013.
- [2] P. Bonacich. Power and centrality: A family of measures. *American journal of sociology*, 92(5):1170–1182, 1987.
- [3] L. Borghesi and C. Milcarek. From B cell to plasma cell. *Immunologic research*, 36(1-3):27–32, 2006.
- [4] F. Breedveld. Therapeutic monoclonal antibodies. *The Lancet*, 355(9205):735–740, 2000.
- [5] Z. Cang, L. Mu, and G.-W. Wei. Representability of algebraic topology for biomolecules in machine learning based scoring and virtual screening. *PLoS computational biology*, 14(1):e1005929, 2018.
- [6] X. Cao. COVID-19: immunopathology and its implications for therapy. *Nature reviews immunology*, 20(5):269–270, 2020.
- [7] Y. Cao, B. Su, X. Guo, W. Sun, Y. Deng, L. Bao, Q. Zhu, X. Zhang, Y. Zheng, C. Geng, et al. Potent neutralizing antibodies against SARS-CoV-2 identified by high-throughput single-cell sequencing of convalescent patients’ B cells. *Cell*, 2020.
- [8] L. Chen, J. Xiong, L. Bao, and Y. Shi. Convalescent plasma as a potential therapy for COVID-19. *The Lancet Infectious Diseases*, 20(4):398–400, 2020.
- [9] I. A. Clark. The advent of the cytokine storm. *Immunology and cell biology*, 85(4):271, 2007.
- [10] D. Corti, J. Misasi, S. Mulangu, D. A. Stanley, M. Kanekiyo, S. Wollen, A. Ploquin, N. A. Doria-Rose, R. P. Staupé, M. Bailey, et al. Protective monotherapy against lethal Ebola virus infection by a potentially neutralizing antibody. *Science*, 351(6279):1339–1342, 2016.
- [11] S. Crotty. A brief history of t cell help to B cells. *Nature Reviews Immunology*, 15(3):185–189, 2015.
- [12] D. De Vlieger, M. Ballegeer, I. Rossey, B. Schepens, and X. Saelens. Single-domain antibodies and their formatting to combat viral infections. *Antibodies*, 8(1):1, 2019.
- [13] W. L. DeLano et al. Pymol: An open-source molecular graphics tool. *CCP4 Newsletter on protein crystallography*, 40(1):82–92, 2002.
- [14] M. Diaz and P. Casali. Somatic immunoglobulin hypermutation. *Current opinion in immunology*, 14(2):235–240, 2002.
- [15] M. Dumoulin, K. Conrath, A. Van Meirhaeghe, F. Meersman, K. Heremans, L. G. Frenken, S. Muyl-dermans, L. Wyns, and A. Matagne. Single-domain antibody fragments with high conformational stability. *Protein Science*, 11(3):500–515, 2002.
- [16] H. Edelsbrunner, D. Letscher, and A. Zomorodian. Topological persistence and simplification. In *Proceedings 41st annual symposium on foundations of computer science*, pages 454–463. IEEE, 2000.
- [17] E. Estrada. Quantifying network heterogeneity. *Physical Review E*, 82(6):066102, 2010.
- [18] E. Estrada. Topological analysis of SARS-CoV-2 main protease. *Chaos: An Interdisciplinary Journal of Nonlinear Science*, 30(6):061102, 2020.
- [19] E. Estrada and N. Hatano. Communicability in complex networks. *Physical Review E*, 77(3):036111, 2008.
- [20] E. Estrada and N. Hatano. Communicability angle and the spatial efficiency of networks. *SIAM Review*, 58(4):692–715, 2016.

- [21] E. Estrada and J. A. Rodriguez-Velazquez. Subgraph centrality in complex networks. *Physical Review E*, 71(5):056103, 2005.
- [22] L. J. Fanning, A. M. Connor, and G. E. Wu. Development of the immunoglobulin repertoire. *Clinical immunology and immunopathology*, 79(1):1–14, 1996.
- [23] A. Forsman, E. Beirnaert, M. M. Aasa-Chapman, B. Hoorelbeke, K. Hijazi, W. Koh, V. Tack, A. Szynol, C. Kelly, A. McKnight, et al. Llama antibody fragments with cross-subtype human immunodeficiency virus type 1 (HIV-1)-neutralizing properties and high affinity for HIV-1 gp120. *Journal of virology*, 82(24):12069–12081, 2008.
- [24] L. C. Freeman. Centrality in social networks conceptual clarification. *Social networks*, 1(3):215–239, 1978.
- [25] J. Govaert, M. Pellis, N. Deschacht, C. Vincke, K. Conrath, S. Muyldermans, and D. Saerens. Dual beneficial effect of interloop disulfide bond for single domain antibody fragments. *Journal of Biological Chemistry*, 287(3):1970–1979, 2012.
- [26] G. Hale. Therapeutic antibodies delivering the promise? *Advanced drug delivery reviews*, 58(5-6):633–639, 2006.
- [27] C. Hamers-Casterman, T. Atarhouch, S. Muyldermans, G. Robinson, C. Hammers, E. B. Songa, N. Bendahman, and R. Hammers. Naturally occurring antibodies devoid of light chains. *Nature*, 363(6428):446–448, 1993.
- [28] I. Hamming, W. Timens, M. Bulthuis, A. Lely, G. Navis, and H. van Goor. Tissue distribution of ACE2 protein, the functional receptor for SARS coronavirus. a first step in understanding SARS pathogenesis. *The Journal of Pathology: A Journal of the Pathological Society of Great Britain and Ireland*, 203(2):631–637, 2004.
- [29] L. Hanke, M. L. P. Vidakovics, D. Sheward, H. Das, T. Schulte, A. M. Morro, M. Corcoran, A. Achour, G. K. Hedestam, B. M. Hällberg, et al. An alpaca nanobody neutralizes SARS-CoV-2 by blocking receptor interaction. *BioRxiv*, 2020.
- [30] T. T. Hansel, H. Kropshofer, T. Singer, J. A. Mitchell, and A. J. George. The safety and side effects of monoclonal antibodies. *Nature reviews Drug discovery*, 9(4):325–338, 2010.
- [31] B. Heyman. Complement and Fc-receptors in regulation of the antibody response. *Immunology letters*, 54(2-3):195–199, 1996.
- [32] W. C. Hwang, Y. Lin, E. Santelli, J. Sui, L. Jaroszewski, B. Stec, M. Farzan, W. A. Marasco, and R. C. Liddington. Structural basis of neutralization by a human anti-severe acute respiratory syndrome spike protein antibody, 80R. *Journal of Biological Chemistry*, 281(45):34610–34616, 2006.
- [33] J. Jankauskaitė, B. Jiménez-García, J. Dapkūnas, J. Fernández-Recio, and I. H. Moal. Skempi 2.0: an updated benchmark of changes in protein–protein binding energy, kinetics and thermodynamics upon mutation. *Bioinformatics*, 35(3):462–469, 2019.
- [34] B. Ju, Q. Zhang, J. Ge, R. Wang, J. Sun, X. Ge, J. Yu, S. Shan, B. Zhou, S. Song, et al. Human neutralizing antibodies elicited by SARS-CoV-2 infection. *Nature*, pages 1–8, 2020.
- [35] B. Kelley. Developing therapeutic monoclonal antibodies at pandemic pace. *Nature biotechnology*, 38(5):540–545, 2020.
- [36] G. Köhler and C. Milstein. Continuous cultures of fused cells secreting antibody of predefined specificity. *Nature*, 256(5517):495–497, 1975.

- [37] J. Lan, J. Ge, J. Yu, S. Shan, H. Zhou, S. Fan, Q. Zhang, X. Shi, Q. Wang, L. Zhang, et al. Structure of the SARS-CoV-2 spike receptor-binding domain bound to the ACE2 receptor. *Nature*, pages 1–6, 2020.
- [38] N. S. Laursen, R. H. Friesen, X. Zhu, M. Jongeneelen, S. Blokland, J. Vermond, A. van Eijgen, C. Tang, H. van Diepen, G. Obmolova, et al. Universal protection against influenza infection by a multidomain antibody to influenza hemagglutinin. *Science*, 362(6414):598–602, 2018.
- [39] B. Leader, Q. J. Baca, and D. E. Golan. Protein therapeutics: a summary and pharmacological classification. *Nature reviews Drug discovery*, 7(1):21–39, 2008.
- [40] E. Market and F. N. Papavasiliou. V (D) J recombination and the evolution of the adaptive immune system. *PLoS biology*, 1(1), 2003.
- [41] I. S. Mian, A. R. Bradwell, and A. J. Olson. Structure, function and properties of antibody binding sites. *Journal of molecular biology*, 217(1):133–151, 1991.
- [42] K. Murphy and C. Weaver. *Janeway’s immunobiology*. Garland science, 2016.
- [43] D. D. Nguyen, K. Xia, and G.-W. Wei. Generalized flexibility-rigidity index. *The Journal of chemical physics*, 144(23):234106, 2016.
- [44] A. Nissim and Y. Chernajovsky. Historical development of monoclonal antibody therapeutics. In *Therapeutic Antibodies*, pages 3–18. Springer, 2008.
- [45] J. E. Pak, C. Sharon, M. Satkunarajah, T. C. Auperin, C. M. Cameron, D. J. Kelvin, J. Seetharaman, A. Cochrane, F. A. Plummer, J. D. Berry, et al. Structural insights into immune recognition of the severe acute respiratory syndrome coronavirus S protein receptor binding domain. *Journal of molecular biology*, 388(4):815–823, 2009.
- [46] F. Pedregosa, G. Varoquaux, A. Gramfort, V. Michel, B. Thirion, O. Grisel, M. Blondel, P. Prettenhofer, R. Weiss, V. Dubourg, et al. Scikit-learn: Machine learning in python. *The Journal of machine Learning research*, 12:2825–2830, 2011.
- [47] D. Pinto, Y.-J. Park, M. Beltramello, A. C. Walls, M. A. Tortorici, S. Bianchi, S. Jaconi, K. Culap, F. Zatta, A. De Marco, et al. Structural and functional analysis of a potent sarbecovirus neutralizing antibody. *BioRxiv*, 2020.
- [48] P. Prabakaran, J. Gan, Y. Feng, Z. Zhu, V. Choudhry, X. Xiao, X. Ji, and D. S. Dimitrov. Structure of severe acute respiratory syndrome coronavirus receptor-binding domain complexed with neutralizing antibody. *Journal of Biological Chemistry*, 281(23):15829–15836, 2006.
- [49] L. G. Presta. Molecular engineering and design of therapeutic antibodies. *Current opinion in immunology*, 20(4):460–470, 2008.
- [50] F. W. Putnam, Y. Liu, and T. Low. Primary structure of a human IgA1 immunoglobulin. IV. streptococcal IgA1 protease, digestion, Fab and Fc fragments, and the complete amino acid sequence of the alpha 1 heavy chain. *Journal of Biological Chemistry*, 254(8):2865–2874, 1979.
- [51] J. V. Ravetch and S. Bolland. IgG fc receptors. *Annual review of immunology*, 19(1):275–290, 2001.
- [52] J. M. Reichert and M. C. Dewitz. Anti-infective monoclonal antibodies: perils and promise of development. *Nature Reviews Drug Discovery*, 5(3):191–195, 2006.
- [53] J. M. Reichert, C. J. Rosensweig, L. B. Faden, and M. C. Dewitz. Monoclonal antibody successes in the clinic. *Nature biotechnology*, 23(9):1073–1078, 2005.

- [54] T. F. Rogers, F. Zhao, D. Huang, N. Beutler, A. Burns, W.-t. He, O. Limbo, C. Smith, G. Song, J. Woehl, et al. Rapid isolation of potent SARS-CoV-2 neutralizing antibodies and protection in a small animal model. *BioRxiv*, 2020.
- [55] M. Rotman, M. M. Welling, M. L. van den Boogaard, L. G. Moursel, L. M. van der Graaf, M. A. van Buchem, S. M. van der Maarel, and L. van der Weerd. Fusion of hIgG1-Fc to <sup>111</sup>In-anti-amyloid single domain antibody fragment VHH-pa2H prolongs blood residential time in APP/PS1 mice but does not increase brain uptake. *Nuclear medicine and biology*, 42(8):695–702, 2015.
- [56] J. F. Scheid, H. Mouquet, N. Feldhahn, M. S. Seaman, K. Velinzon, J. Pietzsch, R. G. Ott, R. M. Anthony, H. Zebroski, A. Hurley, et al. Broad diversity of neutralizing antibodies isolated from memory B cells in HIV-infected individuals. *Nature*, 458(7238):636–640, 2009.
- [57] C. Shen, Z. Wang, F. Zhao, Y. Yang, J. Li, J. Yuan, F. Wang, D. Li, M. Yang, L. Xing, et al. Treatment of 5 critically ill patients with COVID-19 with convalescent plasma. *Jama*, 323(16):1582–1589, 2020.
- [58] R. Shi, C. Shan, X. Duan, Z. Chen, P. Liu, J. Song, T. Song, X. Bi, C. Han, L. Wu, et al. A human neutralizing antibody targets the receptor binding site of SARS-CoV-2. *Nature*, pages 1–8, 2020.
- [59] J. Sui, W. Li, A. Murakami, A. Tamin, L. J. Matthews, S. K. Wong, M. J. Moore, A. S. C. Tallarico, M. Olurinde, H. Choe, et al. Potent neutralization of severe acute respiratory syndrome (SARS) coronavirus by a human mAb to S1 protein that blocks receptor association. *Proceedings of the National Academy of Sciences*, 101(8):2536–2541, 2004.
- [60] J. Ter Meulen, E. N. Van Den Brink, L. L. Poon, W. E. Marissen, C. S. Leung, F. Cox, C. Y. Cheung, A. Q. Bakker, J. A. Bogaards, E. Van Deventer, et al. Human monoclonal antibody combination against SARS coronavirus: synergy and coverage of escape mutants. *PLoS medicine*, 3(7), 2006.
- [61] J. D. Thompson, T. J. Gibson, and D. G. Higgins. Multiple sequence alignment using ClustalW and ClustalX. *Current protocols in bioinformatics*, (1):2–3, 2003.
- [62] X. Tian, C. Li, A. Huang, S. Xia, S. Lu, Z. Shi, L. Lu, S. Jiang, Z. Yang, Y. Wu, et al. Potent binding of 2019 novel coronavirus spike protein by a SARS coronavirus-specific human monoclonal antibody. *Emerging microbes & infections*, 9(1):382–385, 2020.
- [63] S. M. C. Tirado and K.-J. Yoon. Antibody-dependent enhancement of virus infection and disease. *Viral immunology*, 16(1):69–86, 2003.
- [64] M. A. Tortorici and D. Veisler. Structural insights into coronavirus entry. *Advances in virus research*, 105:93–116, 2019.
- [65] R. Van der Linden, L. Frenken, B. De Geus, M. Harmsen, R. Ruuls, W. Stok, L. De Ron, S. Wilson, P. Davis, and C. Verrips. Comparison of physical chemical properties of llama VHH antibody fragments and mouse monoclonal antibodies. *Biochimica et Biophysica Acta (BBA)-Protein Structure and Molecular Enzymology*, 1431(1):37–46, 1999.
- [66] H. Waldmann and G. Hale. Campath: from concept to clinic. *Philosophical Transactions of the Royal Society B: Biological Sciences*, 360(1461):1707–1711, 2005.
- [67] A. C. Walls, Y.-J. Park, M. A. Tortorici, A. Wall, A. T. McGuire, and D. Veisler. Structure, function, and antigenicity of the SARS-CoV-2 spike glycoprotein. *Cell*, 2020.
- [68] A. C. Walls, M. A. Tortorici, B.-J. Bosch, B. Frenz, P. J. Rottier, F. DiMaio, F. A. Rey, and D. Veisler. Cryo-electron microscopy structure of a coronavirus spike glycoprotein trimer. *Nature*, 531(7592):114–117, 2016.

- [69] A. C. Walls, M. A. Tortorici, J. Snijder, X. Xiong, B.-J. Bosch, F. A. Rey, and D. Veesler. Tectonic conformational changes of a coronavirus spike glycoprotein promote membrane fusion. *Proceedings of the National Academy of Sciences*, 114(42):11157–11162, 2017.
- [70] A. C. Walls, X. Xiong, Y.-J. Park, M. A. Tortorici, J. Snijder, J. Quispe, E. Cameroni, R. Gopal, M. Dai, A. Lanzavecchia, et al. Unexpected receptor functional mimicry elucidates activation of coronavirus fusion. *Cell*, 176(5):1026–1039, 2019.
- [71] J. Wan, S. Xing, L. Ding, Y. Wang, D. Zhu, B. Rong, S. Wang, K. Chen, C. He, S. Yuan, et al. Human igg neutralizing monoclonal antibodies block SARS-CoV-2 infection. 2020.
- [72] K. Wang, W. Chen, Y.-S. Zhou, J.-Q. Lian, Z. Zhang, P. Du, L. Gong, Y. Zhang, H.-Y. Cui, J.-J. Geng, et al. SARS-CoV-2 invades host cells via a novel route: CD147-spike protein. *BioRxiv*, 2020.
- [73] L. Wang, W. Shi, J. D. Chappell, M. G. Joyce, Y. Zhang, M. Kanekiyo, M. M. Becker, N. van Doremalen, R. Fischer, N. Wang, et al. Importance of neutralizing monoclonal antibodies targeting multiple antigenic sites on the middle east respiratory syndrome coronavirus spike glycoprotein to avoid neutralization escape. *Journal of virology*, 92(10):e02002–17, 2018.
- [74] M. Wang, Z. Cang, and G.-W. Wei. A topology-based network tree for the prediction of protein–protein binding affinity changes following mutation. *Nature Machine Intelligence*, 2(2):116–123, 2020.
- [75] A. M. Waterhouse, J. B. Procter, D. M. Martin, M. Clamp, and G. J. Barton. Jalview version 2: a multiple sequence alignment editor and analysis workbench. *Bioinformatics*, 25(9):1189–1191, 2009.
- [76] D. J. Watts and S. H. Strogatz. Collective dynamics of “small-world” networks. *Nature*, 393(6684):440, 1998.
- [77] J. M. Woof and D. R. Burton. Human antibody–Fc receptor interactions illuminated by crystal structures. *Nature Reviews Immunology*, 4(2):89–99, 2004.
- [78] D. Wrapp, D. De Vlieger, K. S. Corbett, G. M. Torres, N. Wang, W. Van Breedam, K. Roose, L. van Schie, V.-C. COVID, M. Hoffmann, et al. Structural basis for potent neutralization of betacoronaviruses by single-domain camelid antibodies. *Cell*, 2020.
- [79] D. Wrapp, N. Wang, K. S. Corbett, J. A. Goldsmith, C.-L. Hsieh, O. Abiona, B. S. Graham, and J. S. McLellan. Cryo-EM structure of the 2019-nCoV spike in the prefusion conformation. *Science*, 367(6483):1260–1263, 2020.
- [80] C. Wu, Y. Liu, Y. Yang, P. Zhang, W. Zhong, Y. Wang, Q. Wang, Y. Xu, M. Li, X. Li, et al. Analysis of therapeutic targets for SARS-CoV-2 and discovery of potential drugs by computational methods. *Acta Pharmaceutica Sinica B*, 2020.
- [81] F. Wu, S. Zhao, B. Yu, Y.-M. Chen, W. Wang, Z.-G. Song, Y. Hu, Z.-W. Tao, J.-H. Tian, Y.-Y. Pei, et al. A new coronavirus associated with human respiratory disease in China. *Nature*, 579(7798):265–269, 2020.
- [82] Y. Wu, F. Wang, C. Shen, W. Peng, D. Li, C. Zhao, Z. Li, S. Li, Y. Bi, Y. Yang, et al. A noncompeting pair of human neutralizing antibodies block COVID-19 virus binding to its receptor ACE2. *Science*, 2020.
- [83] K. Xia, K. Opron, and G.-W. Wei. Multiscale multiphysics and multidomain models flexibility and rigidity. *The Journal of chemical physics*, 139(19):11B614.1, 2013.
- [84] L. C. Xue, J. P. Rodrigues, P. L. Kastiris, A. M. Bonvin, and A. Vangone. Prodigy: a web server for predicting the binding affinity of protein–protein complexes. *Bioinformatics*, 32(23):3676–3678, 2016.
- [85] M. Yuan, N. C. Wu, X. Zhu, C.-C. D. Lee, R. T. So, H. Lv, C. K. Mok, and I. A. Wilson. A highly conserved cryptic epitope in the receptor binding domains of SARS-CoV-2 and SARS-CoV. *Science*, 368(6491):630–633, 2020.



- [86] P. Zhou, X.-L. Yang, X.-G. Wang, B. Hu, L. Zhang, W. Zhang, H.-R. Si, Y. Zhu, B. Li, C.-L. Huang, et al. A pneumonia outbreak associated with a new coronavirus of probable bat origin. *Nature*, 579(7798):270–273, 2020.